

ARTICLE

Open Access

Nimbolide protects against endotoxin-induced acute respiratory distress syndrome by inhibiting TNF- α mediated NF- κ B and HDAC-3 nuclear translocation

Venkatesh Pooladanda¹, Sowjanya Thatikonda¹, Swarna Bale¹, Bijay Pattnaik², Dilep Kumar Sigalapalli³, Nagendra Babu Bathini³, Shashi Bala Singh¹ and Chandraiah Godugu¹

Abstract

Acute respiratory distress syndrome (ARDS) is characterized by an excessive acute inflammatory response in lung parenchyma, which ultimately leads to refractory hypoxemia. One of the earliest abnormalities seen in lung injury is the elevated levels of inflammatory cytokines, among them, the soluble tumor necrosis factor (TNF- α) has a key role, which exerts cytotoxicity in epithelial and endothelial cells thus exacerbates edema. The bacterial lipopolysaccharide (LPS) was used both in vitro (RAW 264.7, THP-1, MLE-12, A549, and BEAS-2B) and in vivo (C57BL/6 mice), as it activates a plethora of overlapping inflammatory signaling pathways involved in ARDS. Nimbolide is a chemical constituent of *Azadirachta indica*, which contains multiple biological properties, while its role in ARDS is elusive. Herein, we have investigated the protective effects of nimbolide in abrogating the complications associated with ARDS. We showed that nimbolide markedly suppressed the nitrosative-oxidative stress, inflammatory cytokines, and chemokines expression by suppressing iNOS, myeloperoxidase, and nitrotyrosine expression. Moreover, nimbolide mitigated the migration of neutrophils and mast cells whilst normalizing the LPS-induced hypothermia. Also, nimbolide modulated the expression of epigenetic regulators with multiple HDAC inhibitory activity by suppressing the nuclear translocation of NF- κ B and HDAC-3. We extended our studies using molecular docking studies, which demonstrated a strong interaction between nimbolide and TNF- α . Additionally, we showed that treatment with nimbolide increased GSH, Nrf-2, SOD-1, and HO-1 protein expression; concomitantly abrogated the LPS-triggered TNF- α , p38 MAPK, mTOR, and GSK-3 β protein expression. Collectively, these results indicate that TNF- α -regulated NF- κ B and HDAC-3 crosstalk was ameliorated by nimbolide with promising anti-nitrosative, antioxidant, and anti-inflammatory properties in LPS-induced ARDS.

Introduction

Acute respiratory distress syndrome (ARDS) is a life-threatening disease caused by shock, sepsis, and pneumonia, which eventually culminates into multiple organ failure¹. ARDS is one of the major cause of morbidity and mortality across the world and the epidemiological data suggest that there are 18–79 ARDS cases among 1,00,000 persons per year². Indeed, there is a certain scope to treat infectious lung diseases for reducing the mortality rate³. Lipopolysaccharide (LPS) binds to its cognate Toll-like

Correspondence: Chandraiah Godugu (chandragodugu@gmail.com)

¹Department of Regulatory Toxicology, National Institute of Pharmaceutical Education and Research (NIPER), Balanagar, Hyderabad, Telangana 500037, India

²Centre of Excellence in Asthma & Lung Disease and Molecular Immunogenetics Laboratory, CSIR-Institute of Genomics and Integrative Biology, 110007 New Delhi, India

Full list of author information is available at the end of the article.

Edited by A. Stephanou

© The Author(s) 2019

 **Open Access** This article is licensed under a Creative Commons Attribution 4.0 International License, which permits use, sharing, adaptation, distribution and reproduction in any medium or format, as long as you give appropriate credit to the original author(s) and the source, provide a link to the Creative Commons license, and indicate if changes were made. The images or other third party material in this article are included in the article's Creative Commons license, unless indicated otherwise in a credit line to the material. If material is not included in the article's Creative Commons license and your intended use is not permitted by statutory regulation or exceeds the permitted use, you will need to obtain permission directly from the copyright holder. To view a copy of this license, visit <http://creativecommons.org/licenses/by/4.0/>.

receptor-4 (TLR-4) and the co-receptor cluster of differentiation 14 (CD14) results in lung parenchymal damage, neutrophil accumulation in the interstitial and alveolar compartments, elevated vascular permeability, provocation of pulmonary edema and fibrin deposition^{4,5}. LPS stimulation initiates multiple molecular intracellular signaling events, including classical nuclear factor- κ B (NF- κ B) activation, thereby promoting translocation into the nucleus, thus release inflammatory cytokines principally interleukins (IL-1 β , IL-2, and IL-6) and chemokines (macrophage inflammatory proteins, MIP-1 α/β)⁶. On the other side, TLR-4 activation enhances the tumor necrosis factor- α (TNF- α) production, which is a pleiotropic cytokine of the TNF superfamily involves in the pathogenesis of various inflammatory diseases by inducing the oxidative stress, while depleting antioxidant levels⁷. Therefore, either suppressing the TNF- α secretion or obstruction its biological actions by pharmacological modulators might have eminent therapeutic potential in treating various inflammatory lung diseases⁸.

Histone deacetylases (HDACs) play a crucial role in various diseases, including cancer, diabetes, cardiovascular, neurological, and inflammatory diseases. HDACs are of different classes, among them, HDAC-1 has an important role in inflammatory diseases, where it was found to negatively regulate the inflammatory signaling to repress the expression of NF- κ B regulated genes. Whereas, HDAC-2 does not involve in the NF- κ B signaling directly, but it regulates the NF- κ B activity in association with HDAC-1⁹. On the other side, it was reported that HDAC-1 inhibition in intestinal epithelial cells leads to an increase in p65 NF- κ B phosphorylation and nuclear localization¹⁰. The role of HDAC-3 was extensively studied by Elisabeth Ziesché et al. and revealed its importance as a co-activator in IL-1-induced inflammatory signaling mediated by the removal of inhibitory acetyl groups from p65 NF- κ B¹¹. Similarly, Niek GJ Leus et al. used RGFP966 (HDAC-3 selective inhibitor) in pulmonary inflammation model and found reduced NF- κ B transcription with a reduction in the expression of IL-1 β , IL-6, and IL-12b cytokines in macrophages and found an increase in the expression of the anti-inflammatory cytokine IL-10¹²; while HDAC-4 involves in ROS generation via enhanced vascular cell adhesion protein 1 (VCAM-1) expression¹³. Collectively, it infers that HDAC inhibitors maintain the balance between pro- and anti-inflammatory gene expression, thereby suppress the lung inflammation^{14,15}. Thus, HDAC inhibitors have profound scope in treating various inflammatory diseases.

Nimbolide, a natural chemical constituent isolated from the leaves and flowers of neem (*Azadirachta indica*). It manifested assorted biological activities, including antimalarial, antibacterial, anticancer, and anti-inflammatory activities¹⁶. In the current study, to our knowledge, we

show for the first time the therapeutic potential and molecular mechanism of nimbolide in LPS-induced ARDS-associated pleural inflammation in mice and the underlying molecular inflammatory events were recapitulated in cultured macrophages and lung epithelial cells. Notably, our data demonstrate that nimbolide selectively suppressed I κ B- α -regulated p65 NF- κ B and HDAC-3 crosstalk by inhibiting TNF- α in LPS-induced ARDS.

Materials and methods

Materials

Nimbolide was purchased from Aptus therapeutics, Hyderabad, India. TNF- α recombinant protein was purchased from Thermo Fisher Scientific, USA. LPS from *Escherichia coli* (055: B5), and phorbol 12-myristate 13-acetate (PMA), 3-(4,5-Dimethylthiazol-2-yl)-2,5-Diphenyltetrazolium Bromide (MTT), dimethyl sulfoxide (DMSO), Griess reagent, 2',7'-dichlorofluorescin diacetate (DCFDA), 4', 6'-diamidino-2-phenylindole (DAPI), ethylenediaminetetraacetic acid (EDTA), hematoxylin, eosin, toulidine blue (TB), Ehrlich reagent, Giemsa stain, reduced glutathione (GSH), bovine serum albumin (BSA), sodium dodecyl sulphate (SDS), glacial acetic acid, sodium nitrite and bicinchoninic acid (BCA) reagent were purchased from Sigma-Aldrich, USA. Anti-nitrotyrosine, anti-Nrf-2, anti-SOD-1, anti-HO-1, anti-TNF- α , anti-PCNA, and anti- β -Actin antibodies were purchased from Santa Cruz Biotechnology, USA. Anti-iNOS antibody was purchased from Sigma-Aldrich, USA. Anti-p-NF- κ B (p-p65), anti-NF- κ B (p65), anti-p-IKK α/β , anti-p-I κ B, anti-I κ B, anti-p-MAPK p38, anti-MAPK p38, anti-p-GSK-3 β , anti-GSK-3 β , anti-mTOR, anti-HDAC-1, anti-HDAC-2, anti-HDAC-3, anti-HDAC-4, and anti-H3 antibodies were purchased from Cell Signaling Technologies, USA. Anti-MPO antibody was purchased from PathnSitu Biotechnologies, USA. All secondary anti-rabbit, anti-goat, and anti-mouse antibodies were purchased from Santa Cruz Biotechnology, USA. TNF- α siRNA was purchased from Dharmacon™, USA. All other chemicals were of analytical grade and obtained commercially.

Cell culture

RAW 264.7 (murine macrophages) and A549 (human type II alveolar epithelial cells) cells were obtained from National Centre for Cell Science (NCCS), Pune, India. These cell lines were cultured in appropriate Dulbecco's Modified Eagle's medium (DMEM) and Roswell Park Memorial Institute medium (RPMI-1640) (Invitrogen, USA), respectively. MLE-12 (mouse lung epithelial cells) and BEAS-2B (human bronchial lung epithelial cells) cell lines were procured from American Type Culture Collection (ATCC), USA and cultured in 1:1 ratio of low glucose DMEM and Ham's F-12K (Kaighn's) medium

(Invitrogen, USA). The human monocytic cell line, THP-1 was a kind gift from Dr. Sanjeev Khosla (Lab of Mammalian Genetics, Centre for DNA Fingerprinting and Diagnostics (CDFD), Hyderabad, India) and these cells were grown in RPMI-1640 medium. All the cells were supplemented with 10% fetal bovine serum and 1% antibiotic-antimycotic solution (Sigma-Aldrich, USA). Cells were grown in a humidified CO₂ incubator at 37 °C temperature. For differentiating the monocytes into macrophages, THP-1 cells were primed with PMA (5 nM) for 48 h.

Measurement of cell viability

Cell viability was determined by MTT assay as described previously with slight modifications¹⁷. Here, the cells were seeded in 96-well plate and treated with nimbulide (0.5–10 μM) for 24 h. Then cells were washed with PBS and MTT (0.5 mg/ml) was added to each well, followed by formazan crystals were solubilized with DMSO and absorbance was measured at 570 nm with the spectrophotometer (Spectra Max, M4 Molecular devices, USA).

Measurement of cellular ROS levels

The ROS levels were measured by DCFDA (Sigma-Aldrich, USA) and MitoSOX Red (Invitrogen, USA) fluorescent dyes. For the flow cytometric analysis, RAW 264.7 and differentiated THP-1 cells (1×10^5 cells/well) were seeded in 6-well plate. At 80 % confluence, cells were pre-treated with nimbulide (0.5 and 1 μM) for 24 h. Then cells were stimulated with LPS (1 μg/ml) for 30 min to induce oxidative stress. Later, these cells were further incubated with 10 μM of DCFDA and 5 μM of MitoSOX Red reagent for 15 and 30 min, respectively. After trypsinization, cells were subjected to flow cytometric analysis (BD Accuri C6 flow cytometer, USA) and relative geometric mean was measured. For visualization of apparent changes, cells were observed under Nikon Eclipse inverted fluorescent microscope, (Japan) at $\times 200$ magnification immediately following dye exposure. The fluorescence intensity was measured using a multimode plate reader.

Immunofluorescence (IF)

After LPS or TNF-α stimulation, cells were washed with PBS and fixed with 4% paraformaldehyde for 5 min at room temperature. Then cells were washed and permeabilized with 0.1% Triton-X. Further, the cells were incubated with blocking buffer (3% BSA) for 1 h and probed with primary antibody overnight at 4 °C. Cells were washed and incubated with secondary antibody for 1 h at room temperature. The primary antibodies and secondary antibodies conjugated to FITC or rhodamine (Sigma-Aldrich, USA) used at 1:200 dilutions. The nuclei were visualized with DAPI staining. The coverslips were mounted on to the chamber glass slides with

Fluoroshield™ histology mounting medium (Sigma-Aldrich, USA). Images of the stained slides were captured by Leica TCS SP8 Laser Scanning Spectral Confocal Microscope (Germany).

HDAC fluorometric assay

HDAC levels upon nimbulide treatment (0.05, 0.1, 1, and 2.5 μM) were determined by Histone Deacetylase Assay Kit, Fluorometric (Sigma-Aldrich, USA) according to manufacturer instructions. The HDAC inhibitor, Trichostatin A was used to compare the nimbulide HDAC inhibitory activity from the standard curve.

Animals

Male C57BL/6 mice (8 weeks old) were utilized for the experiment and maintained with 12 h dark/light cycle in an animal house at ambient conditions. Mice were acclimatized for 1 week before the study and given free access to food and water *ad libitum*. All the animal studies were conducted under the due endorsement of Institutional Animal Ethics Committee (IAEC) of National Institute of Pharmaceutical Educational and Research (NIPER), Hyderabad, India, as per the Committee for the Purpose of Control and Supervision of Experiments on Animals (CPCSEA) guidelines of Government of India.

ARDS animal model

Mice were randomly divided into seven groups ($n = 8$): Control, LPS alone (50 μg per mice), LPS + Nimbulide pre-treatment (0.3, 1 and 3 mg/kg), nimbulide alone (3 mg/kg), and concurrent nimbulide treatment group (3 mg/kg nimbulide was given through intraperitoneal (i.p.) administration immediately followed by LPS oropharyngeal instillation for 12 h). The pre-treatment groups received an i.p. injection of nimbulide (0.3, 1 and 3 mg/kg) for 5 days followed by LPS instillation for 12 h except for nimbulide alone group. An equal volume of vehicle, instead of nimbulide was given to the LPS control group. The animals were anesthetized using ketamine (8 mg/kg), and xylazine (45 mg/kg) i.p. administration. When the anesthesia is attained, the animals were placed on a mouse intubation platform at 60° inclined angle with rubber band running under the upper incisors. The tongue of the mouse was pulled and held with blunt forceps. Then, 50 μg of LPS in 50 μl volume of sterile water for injection was administered into the back of oral cavity using a micro-pipette, the tongue was held until the liquid disappeared from the mouth while the gasping sound is audible as an indication of instillation into lungs.

Changes in body weights, lung weight index, and body temperature

Initially, body weights of animals were taken before administration of nimbulide. After 5 days of nimbulide

pre-treatment, LPS was instilled to the animals for 12 h and again body weights were measured and net body weight changes were calculated. After animal sacrifice, lung weights were noted to determine the lung weight index. Body temperatures were recorded before and after the administration of LPS with a rectal probe attached to the homeothermic monitor (Harvard Apparatus, USA).

Bronchoalveolar lavage (BAL) analysis

Mice were sacrificed and the lungs were lavaged 3 times with 1 ml ice-cold PBS. BAL samples were pooled and centrifuged at 300 × g for 10 min. The cell pellets obtained after centrifugation were resuspended in 1 ml PBS and subjected to differential cell counter ADVIA 2120i Hematology System (Siemens, Germany).

Blood analysis

Blood was collected from mice by cardiac puncture to determine different blood parameters. The blood was collected in heparin solution contained centrifugal tubes. The whole blood was subjected to automatic blood cell analyzer for detailed hematological analysis.

Measurement of nitrite and GSH levels

Nitrite levels were quantified by Griess assay¹⁸, while glutathione levels were measured by Ellman's reagent¹⁹ as described earlier with slight changes.

Multiplex bead-based cytokine assay

After 12 h of LPS treatment, cytokine and chemokine levels were measured in RAW 264.7 cells and lung tissues by Luminex assay based on xMAP technology (MAGPIX, Millipore, Germany). This assay was performed with customized highly sensitive MILLIPLEX MAP Kit (Millipore, Germany) according to the manufacturer's protocol.

Enzyme-linked immune sorbent assay (ELISA)

Expressions of proinflammatory cytokines TNF-α, TGF-β, IL-2, and IL-1β in lung tissue and cell culture supernatants were assessed using commercially available ELISA kits (eBioscience, USA).

Histopathological examination

The 5-micron lung tissue sections were stained with hematoxylin followed by eosin (H&E) and toluidine blue (TB) to observe pathological and morphological changes in the lung tissue. A semiquantitative histopathologic scoring was used to estimate the lung structural and cellular changes. The scoring was given as follows; (1) perivascular neutrophils (0—absent; 1—<10 per high-power field; 2—10–50 per high power field; 3—>50 per high-power field); (2) perivascular hemorrhage (0—absent; 1—patchy and mild; 2—extensive and mild;

3—extensive and marked); (3) neutrophilic margination in medium-sized vessels (0—absent; 1—present). A total inflammatory score (range, 0–7) was taken as the sum of the individual scores and quantified by a histopathologist who was unaware of treatment groups²⁰. Mucosal mast cells were counted in 10 random fields per group as per the previous report²¹.

Immunohistochemistry (IHC)

IHC was performed as per standard protocol reported earlier²². The sections were blocked with immune serum for avoiding non-specific binding. Then sections were incubated with anti-TNF-α, anti-NF-κB, and anti-HDAC-3 primary antibodies overnight at 4 °C. The further procedure was performed with the PolyExcel HRP/DAB Detection System kit (PathnSitu Biotechnologies, USA) and followed the manufacturer instructions. Then immune reactions were visualized by adding the DAB (3,3'-diaminobenzidine tetrachloride) and all sections were counterstained with hematoxylin. The protein expression was quantified by ImageJ Fiji.

Western blot analysis

Whole cell, cytosolic, and nuclear protein isolation was performed as described earlier^{23,24}. Protein concentration was estimated by BCA colorimetric assay kit as per manufacturer guidelines. Samples were loaded and subjected to SDS-PAGE. After electrophoresis, proteins were electrotransferred to nitrocellulose membrane (Bio-Rad, USA) and probed with primary and secondary antibodies before detecting with the enhanced chemiluminescence (ECL) solution (Bio-Rad, USA) by the chemdoc imaging system (Vilber Fusion Fx, France). The densitometric analysis was performed by ImageJ software, NIH, USA. β-Actin and histone H3 were used as internal controls for normalization of cytosolic as well as nuclear proteins.

Real-time PCR

RNA was isolated from lung tissues using RNA isolation kit (Qiagen, Germany). After reverse transcription with Verso cDNA synthesis kit (Applied Biosystems, USA), real-time-PCR was performed on ABI 7500 system (Applied Biosystems, USA) using DyNAmoColourFlash SYBR Green qPCR kit (Thermo Fisher Scientific, USA) followed by the addition of forward and reverse primers (Integrated DNA Technologies, USA). After amplification, a melting-curve analysis was performed to verify the specificity of the reaction. The 18S rRNA gene was used as an internal control and results were determined by $2^{-\Delta\Delta Ct}$. Relative mRNA levels were expressed as the fold change over the normal control. The primer sequences were described in supplementary data (Supplementary Table S1).

In silico molecular docking analysis

The crystal structure of the human TNF- α (PDB ID: 2AZ5)²⁵ was used for molecular docking studies. For the ligand docking, the standard precision mode was selected. Docking was performed by using the standard protocol implemented in Maestro, version 9.7 and the ligands were docked against the active site of the targeted protein. No constraints were defined for the docking runs. The detailed procedure was described in supplementary data.

In vitro macrophage bactericidal activity

Macrophagic bactericidal activity was performed as described previously with slight modifications²⁶. RAW 264.7 cells alone or cells were treated with nimbolide (1 μ M) and incubated in serum-free medium for 24 h. Then cells were stimulated with LPS (1 μ g/ml) and incubated for 12 h. Later, cells were scraped in an ice-cold serum-free medium, washed twice with PBS and re-suspended in serum-free medium in triplicates. Wild-type *Pseudomonas aeruginosa* (Strain number: 424) (Pa) was procured from Microbial Type Culture Collection and Gene Bank, India. Bacteria from the exponential phase were added to the RAW 264.7 cells at a macrophage/bacteria ratio of 1:10. Bacterial phagocytosis was allowed to proceed for 60 min at 37 °C. At the end of the experiment, cells were lysed in 0.1% Triton X-100 solution and bacteria contained supernatant was collected and plated on to the nutrient-agar plates for colony counting to obtain bacterial uptake values. The Pa colonies were counted after 3 days of incubation at 37 °C. The macrophage bactericidal activity was calculated as follows.

$$\% \text{ Pa killed} = (1 - [\text{Pa C60}/\text{Pa C0}]) \times 100.$$

Here,

Pa C60 = Number of Pa colonies after 60 min incubation.

Pa C0 = Number of Pa colonies at the beginning of incubation.

Loss of TNF- α function and nuclear translocation of NF- κ B and HDAC-3

BEAS-2B cells were transfected with TNF- α siRNA to knock down the TNF- α expression. Briefly, cells were seeded in 6-well plates at a density of 1×10^6 /well and cultured for 24 h at 37 °C. After attaining 80% confluence, cells were transfected with TNF- α and scrambled siRNA (50 nM) by Lipofectamine 3000 (Invitrogen, USA) according to the manufacturer instructions. In another set of experiment, cells were treated with nimbolide (2.5 μ M). After 24 h of incubation, the cells were stimulated with 10 ng/ml of TNF- α for 30 min and determined the expression of TNF- α , NF- κ B, and HDAC-3.

Statistical analysis

Results were expressed as mean \pm SEM, and n refers to the number of sample replicates. The statistical differences between the means were determined by one-way ANOVA followed by Tukey's multiple comparison tests with Prism software (version 6.01; GraphPad, USA). $p < 0.05$ was considered to be statistically significant.

Results

Nimbolide reduces the LPS-induced nitrosative and oxidative stress

From the predicted physicochemical properties, it was found that nimbolide exhibited superior drug-likeness properties in terms of absorption, distribution, metabolism, and excretion-toxicity (ADME/T), hence it could be a potential lead molecule for treating various inflammatory diseases (Table S2). In our experiment, cells (RAW 264.7, differentiated THP-1, MLE-12, A549, and BEAS-2B cells) were stimulated with LPS, further induced the oxidative stress and inflammatory signaling cascade. Initially, we performed MTT assay to ascertain the effect of nimbolide on the viability of aforementioned cell lines. Our results revealed that nimbolide had minimal effect on the viability in the tested cell lines up to 2.5 μ M concentrations at 24 h post-treatment (Supplementary Figure S1A–E). Therefore, concentrations up to 2.5 μ M were fixed to execute further molecular mechanistic studies.

Among all nitric oxide synthases (NOSs), iNOS is mainly involved in the inflammatory diseases and further activates various inflammatory cytokines²⁷. As nitrite is the final product of NO, these levels were found to be elevated in LPS stimulated group as compared to normal control (NC), moreover, these levels were significantly reduced by nimbolide in both RAW 264.7 (Fig. 1a) and differentiated THP-1 cells (Fig. 1b). The mechanism behind the downregulation of nitrite levels upon nimbolide treatment was determined by immunoblotting. The increased nitrotyrosine and iNOS proteins expression were observed with LPS stimulation. Furthermore, nimbolide significantly suppressed these nitrosative stress regulators in both RAW 264.7 (Fig. 1c and Supplementary Figure S2A, B and differentiated THP-1 cells (Fig. 1d and Supplementary Figure S2C, D) in a concentration-dependent manner. Similar results were found in mouse lung epithelial cells, where nimbolide inhibited the iNOS expression (Supplementary Figure S3A, B & D).

LPS induces the oxidative stress, which further activates the various inflammatory signaling pathways. Consistently, we observed that LPS induced both intracellular and mitochondrial ROS (mROS) levels, whereas nimbolide treatment (0.5 and 1 μ M) significantly reduced the oxidative stress in both RAW 264.7 (Fig. 1e, f; Supplementary Figures S2E, F and S2I–L) and differentiated

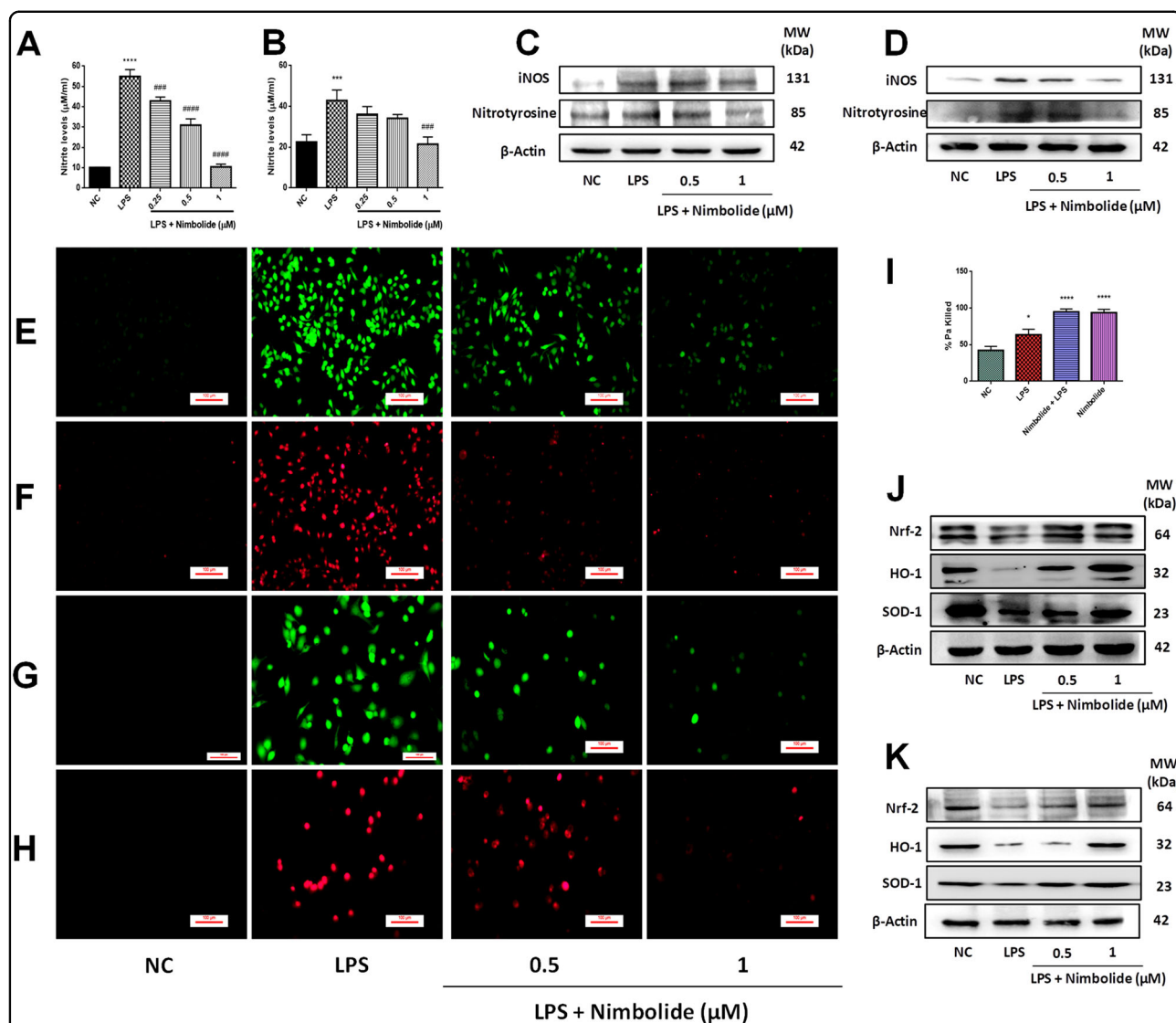


Fig. 1 Nimbulide protects the lungs from nitrosative and oxidative stress. Cells were pre-treated with nimbulide for 24 h and oxidative stress was induced with LPS (1 $\mu\text{g}/\text{ml}$). After 24 h of incubation, the nitrite levels were measured in cell culture supernatants of (a) RAW 264.7 and (b) differentiated THP-1 cells by Griess assay. Whole cell protein was extracted and subjected to western blot and measured the expression of nitrotyrosine and iNOS in both (c) RAW 264.7 and (d) differentiated THP-1 cells. After 30 min of LPS stimulation, intracellular and mitochondrial ROS (mROS) levels were measured by (e, g) DCFDA and (f, h) MitoSOX Red staining in both RAW 264.7 and differentiated THP-1 cells, respectively. The fluorescent images were captured at $\times 200$ magnification from different groups. (i) RAW264.7 cells were pre-treated with nimbulide (1 μM) and oxidative stress was induced by LPS (1 $\mu\text{g}/\text{ml}$). After 12 h of LPS exposure, cells were incubated with Pa and macrophage bactericidal activity was calculated by counting Pa colonies on nutrient agar plates. Western blot was performed to determine the Nrf-2, HO-1, and SOD1 expression in both (j) RAW 264.7 and (k) differentiated THP-1 cells from whole cell lysate. Data represented as mean \pm SEM ($n = 3$ independent experiments). * $P < 0.05$, ** $P < 0.01$, and *** $P < 0.001$ and **** $P < 0.0001$ is significantly different from the normal control (NC) group; ## $P < 0.001$ and ### $P < 0.0001$ are significantly different from the LPS group.

THP-1 cells (Fig. 1g, h; Supplementary Figures S2G, H and S2M-P). The mROS is considered to have a prime role in mediating bactericidal activity, even though nimbulide scavenged mROS but did not impair the bactericidal activity by murine macrophages, moreover, an enhanced antimicrobial activity was observed (Fig. 1i). The nuclear factor erythroid 2-related factor 2 (Nrf-2)

manifests the antioxidant responsive genes that regulate the oxidative stress and maintain the cellular homeostasis through the induction of catabolism of superoxide ions by superoxide dismutase (SOD) and stress response protein, heme oxygenase-1 (HO-1)²⁸. The protein expressions of Nrf-2, SOD1, and HO-1 were significantly enhanced by nimbulide in comparison with LPS control and reduces

the oxidative stress observed in both RAW 264.7 (Fig. 1j and Supplementary Figure S2Q–S) and differentiated THP-1 cells (Fig. 1k and Supplementary Figure S2T–V). Similar results were observed in MLE-12 cells, where nimbolide enhances the Nrf-2 expression (Supplementary Figure S3A, C & E)

Nimbolide normalizes the LPS-induced physiological changes and downregulates the inflammation responsive cells in bronchoalveolar lavage fluid (BALF) and blood

LPS altered the normal physiology with severe pathological changes such as hypothermia and weight loss at 12 h of post exposure. In addition, LPS induced the accumulation of serous fluids in the lungs which resulted in pulmonary edema evident with increased lung weight index. However, nimbolide treatment at 3 mg/kg concentration did not impair the body weights but reduced the abnormal lung weight index. Whereas hypothermia was normalized significantly at all the doses tested (0.3, 1 and 3 mg/kg) (Fig. 2a–c). Previous reports suggest that LPS elevates total cells, white blood cells (WBC), neutrophils, lymphocytes, macrophages, eosinophils and basophils in BALF, which play a key role in propagating inflammation²⁹. Whereas, nimbolide treatment significantly suppressed these cell counts in BALF (Fig. 2d–j).

Similarly, in whole blood analysis, it was found that LPS induced the platelets and absolute neutrophils count along with decreased hemoglobin (Hb) levels, whereas nimbolide intervention did not alter these levels (Fig. 2k–m).

Nimbolide reduces LPS-induced pathological consequences and mast cell infiltration in lung tissues

LPS instilled animal group exhibited severe pathological changes and caused the endothelial barrier dysfunction. As evident from H&E results, it was observed that inflammatory cells such as neutrophils influx into the alveolar spaces, thus led to the thickening of an interalveolar septum (Fig. 3a and Supplementary Figure S4A). Additionally, from TB staining, it was observed that there was a dramatic accumulation and infiltration of a mast cell density (Fig. 3b and Supplementary Figure S4B). Moreover, nimbolide pre-treatment remarkably repressed both pathological consequences at 1 and 3 mg/kg doses. Whereas in concurrent administration at 3 mg/kg, there was no significant reduction observed in comparison to LPS instilled group. However, when nimbolide alone treatment at 3 mg/kg was tested, we did not observe the alveolar structural changes and appeared normal. Hence, further experiments were performed in pre-treatment groups of nimbolide to investigate its molecular mechanism.

Repression of inflammatory signaling responsive cytokines and chemokines by nimbolide in LPS-induced lung injury

We performed multiplex analysis to determine the cytokine and chemokine levels. We observed elevated proinflammatory cytokines such as IL-1 β , IL-6, IL-12 (p40), TNF- α , TGF- β , and chemokines (MIP-1 α and MIP-1 β) with reduced levels of anti-inflammatory cytokines including IL-4, IL-10, and IL-13 were observed in LPS treated groups³⁰. Furthermore, nimbolide significantly reduced the proinflammatory cytokines and chemokines, concomitantly induced the anti-inflammatory cytokines in lung tissues (Fig. 4a–h), respectively. To further confirm with the multiplex results, we performed ELISA to investigate the expression of cytokines including IL-1 β and TGF- β in lung tissues (Fig. 4i, j), where LPS driven cytokine levels were significantly reduced by nimbolide which is consistent with multiplex results. Additionally, these cytokines and chemokine levels were analyzed in RAW 264.7 and A549 cells, where nimbolide pre-treatment significantly inhibited the cytokine-mediated inflammation (Supplementary Figure S5). The anti-inflammatory activity of nimbolide was mediated by suppressing the LPS-induced nitrite levels with a simultaneous increase in GSH levels (Fig. 4k, l). Moreover, LPS induces the oxidative and nitrosative stress via myeloperoxidase (MPO), iNOS and nitrotyrosine, which was significantly decreased by nimbolide through the upregulation of antioxidative regulators such as Nrf-2, SOD-1, and HO-1 expression (Fig. 4m, n and Supplementary Figure S6a–f).

Nimbolide inhibits TNF- α mediated pulmonary inflammation

As evident from ELISA and multiplex results, nimbolide was found to have a key role in inhibiting TNF- α . These results prompted us to decipher the molecular interactions of nimbolide with TNF- α , hence docking studies were performed. The results of molecular docking along with hydrogen bonding as well as hydrophobic interactions of ligands with TNF- α were depicted in Table S3. The docking results illustrated the predicted binding modes and the detailed protein inhibitor interactions of nimbolide with TNF- α . From the molecular docking analysis, it was observed that nimbolide established two hydrogen bonds between the methyl ester group of the compound and the active site residues (Leu120 and Ser60) of TNF- α . Additionally, the furan ring of the compound formed a π - π stacking interaction (arene-arene interaction) with Tyr59. Furthermore, several hydrophobic interactions were found between nimbolide and active site residues, e.g., Leu57, Tyr59, Tyr119, Leu120, Val123, Tyr151, and Ile155 are the other residues that stabilized the binding of nimbolide in the active site of TNF- α . The binding model of nimbolide also revealed that they share

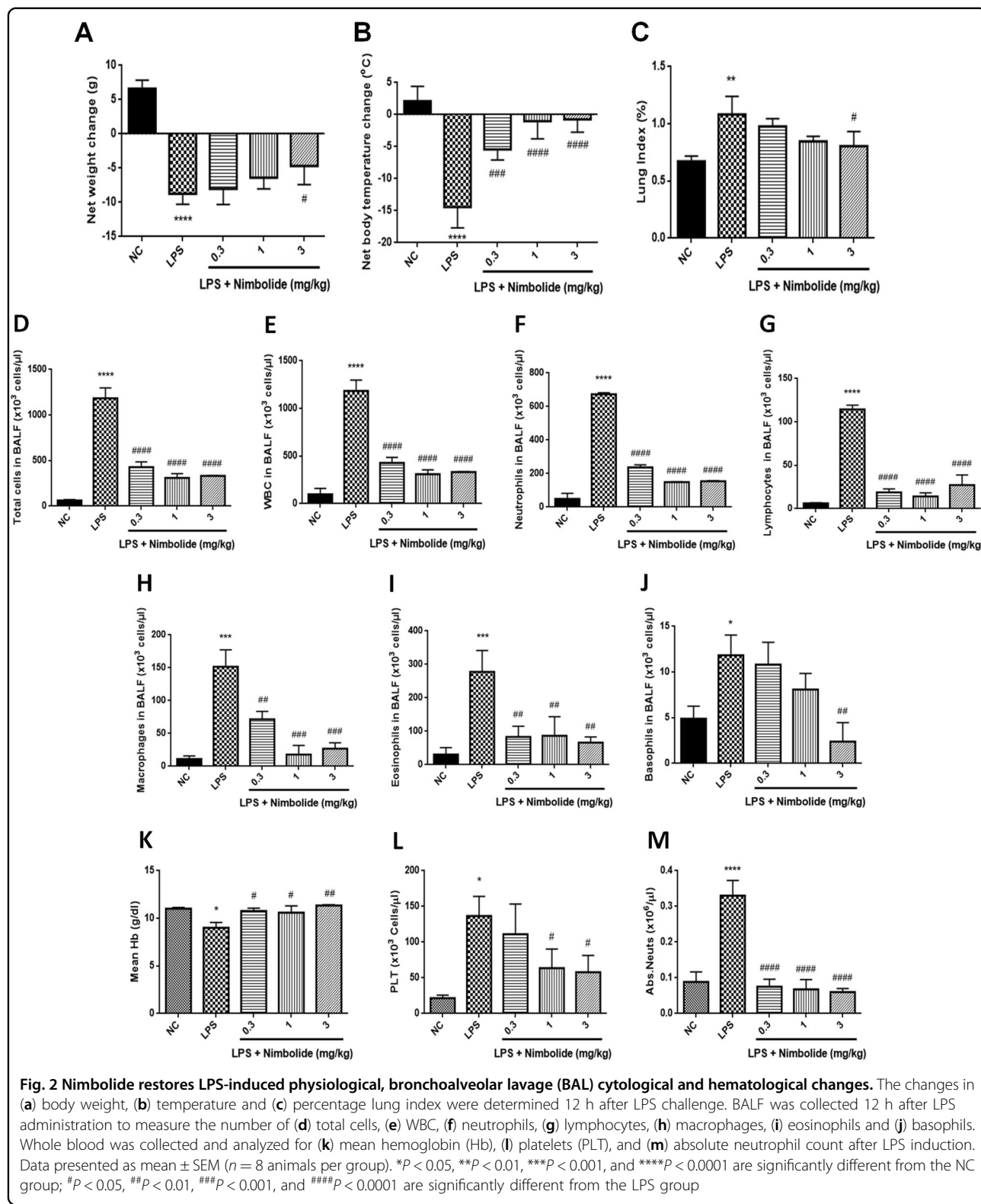
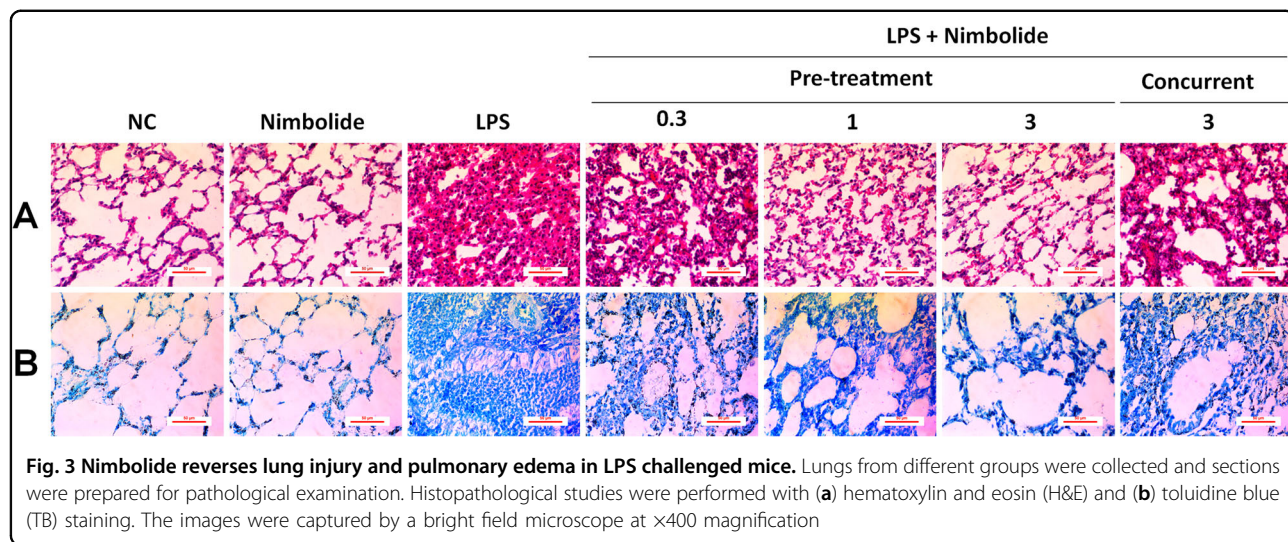


Fig. 2 Nimbolide restores LPS-induced physiological, bronchoalveolar lavage (BAL) cytological and hematological changes. The changes in (a) body weight, (b) temperature and (c) percentage lung index were determined 12 h after LPS challenge. BALF was collected 12 h after LPS administration to measure the number of (d) total cells, (e) WBC, (f) neutrophils, (g) lymphocytes, (h) macrophages, (i) eosinophils and (j) basophils. Whole blood was collected and analyzed for (k) mean hemoglobin (Hb), (l) platelets (PLT), and (m) absolute neutrophil count after LPS induction. Data presented as mean \pm SEM ($n = 8$ animals per group). * $P < 0.05$, ** $P < 0.01$, *** $P < 0.001$, and **** $P < 0.0001$ are significantly different from the NC group; # $P < 0.05$, ## $P < 0.01$, ### $P < 0.001$, and ##### $P < 0.0001$ are significantly different from the LPS group

one common hydrogen bonding and arene-arene interactions with the key residues of the active site as shown by co-crystallized ligand. Moreover, docked nimbolide and

co-crystallized ligand suggested that nimbolide also occupies the binding pocket in a similar fashion to that of co-crystallized ligand (Fig. 5a, b). To further affirm these



results, we extensively analyzed the effect of nimbolide on TNF- α expression. Collectively, the confocal (Fig. 5c) and IHC (Fig. 5d and Supplementary Figure S7A) results unveiled that nimbolide significantly decreased the LPS-induced TNF- α expression at translational level.

We further investigated the role of nimbolide on TNF- α mediated downstream inflammatory signaling pathways, where nimbolide markedly inhibited the LPS-induced phosphorylation of TNF- α regulated p38 MAPK, IKK- α/β , I κ B- α , p65 NF- κ B, GSK-3 β along with mTOR expression in A549 cells (Fig. 5e and Supplementary Figure S7B–H) as well as lung tissues (Fig. 5f and Supplementary Figure S7I–O). Further, it is our interest to explore the effect of nimbolide on epigenetic alterations which are commonly associated with LPS in inflammatory conditions. Here, we found aberrant expression of HDAC-1, 2, 3, and 4 upon LPS stimulation. Interestingly, nimbolide repressed the HDACs expression in a dose-dependent manner in vitro (A549 cells; Fig. 5g and Supplementary Figure S7P–S) and the results were consistent with in vivo (Fig. 5h and Supplementary Figure S7T–W). To confirm the HDAC inhibitory activity of nimbolide, we performed a fluorimetric based HDAC assay. Where, we found that there was a significant reduction in HDAC levels by nimbolide at different concentrations such as 0.05, 0.1, 1, and 2.5 μ M, where the HDAC levels were 0.44 ± 0.06 , 0.49 ± 0.13 , 0.26 ± 0.03 , and 0.24 ± 0.01 μ M, respectively in comparison with trichostatin A, which inhibited the HDAC levels up to 0.52 ± 0.02 μ M at 2.5 μ M concentration (Fig. 5i).

Nimbulide inhibits NF- κ B and HDAC-3 nuclear translocation

The western blot analysis results inferred that LPS stimulation significantly enhanced the translocation of NF- κ B and HDAC-3 into the nucleus, whereas nimbulide

treatment hindered the nuclear translocation, where NF- κ B and HDAC-3 were confined to the cytoplasm (Fig. 6a, b and Supplementary Figure S8A–D). For further confirmation of nimbulide inhibitory mechanism of nuclear translocation, we performed IF to examine the effect of nimbulide on NF- κ B and HDAC-3 expression. Here, nimbulide significantly inhibited the NF- κ B and HDAC-3 expression and co-localization in contrast to LPS treatment in A549 cells (Fig. 6c). The similar pattern of decreased expression was observed by IHC, where LPS surged the NF- κ B and HDAC-3 protein expression. Further treatment with nimbulide repressed the protein expression by truncating the immunopositivity against LPS-induced alveolar inflammation (Fig. 6d and Supplementary Figure S8E, F). Additionally, nimbulide significantly attenuated the LPS-induced TNF- α , NF- κ B, and HDAC-3 mRNA levels at transcriptional level studied by RT-PCR (Supplementary Figure S9).

Consistent with LPS activity, we observed TNF- α induced the nuclear translocation of NF- κ B and HDAC-3, whereas nimbulide significantly reduced this effect in A549 cells confirmed by western blotting (Fig. 7a and Supplementary Figure S10A–D) and IF analysis (Fig. 7b). Additionally, we evaluated the role of nimbulide in TNF- α -mediated NF- κ B and HDAC-3 nuclear translocation in bronchial epithelial cells. TNF- α expression was silenced by siRNA and nuclear NF- κ B and HDAC-3 levels were examined, where TNF- α siRNA treated groups did not exhibit the nuclear translocation of NF- κ B and HDAC-3, which further confirms that TNF- α is essential for activating the inflammatory cascade through nuclear translocation in ARDS. Moreover, nimbulide significantly reduced the nuclear translocation and showed similar results as TNF- α siRNA treated group, which was confirmed by both immunoblotting (Fig. 7c and Supplementary Figure S10E–G) and

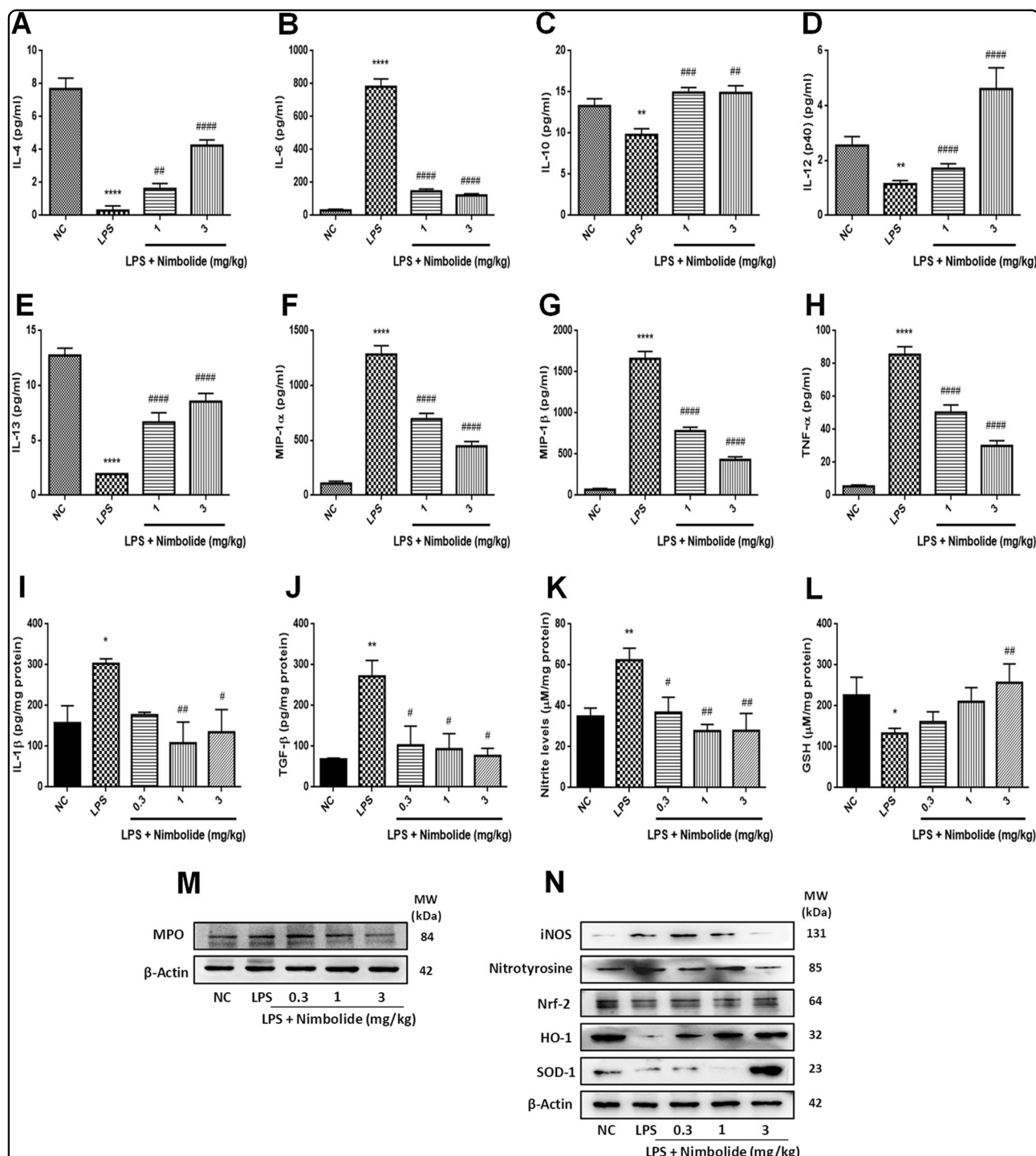


Fig. 4 Nimbolide modulates the pro- and anti-inflammatory cytokines and chemokines. The proinflammatory cytokines and chemokines (IL-6, IL-12(p40), MIP-1 α , MIP-1 β , and TNF- α) and anti-inflammatory cytokines (IL-4, IL-10, and IL-13) expression were determined by multiplex and ELISA. **a-h** Animal lung tissue lysate was prepared and evaluated for the levels of aforementioned inflammatory cytokines and chemokines by multiplex. **i-j** Lung tissue supernatants were subjected to ELISA to determine IL-1 β and TGF- β cytokines expression. **k** Griess assay was performed to determine the nitrite levels in cell lysate of lung tissues. **l** The antioxidant GSH levels were measured in lung tissue. **m** The MPO as well as **(n)** iNOS, nitrotyrosine, Nrf-2, HO-1, and SOD-1 protein expressions were determined by immunoblot analysis. Data presented as mean \pm SEM (n=8 mice per group). *P < 0.05, **P < 0.01, and ****P < 0.0001 are significantly different from the NC group; #P < 0.05, ##P < 0.01, ###P < 0.001, and #####P < 0.0001 are significantly different from the LPS group.

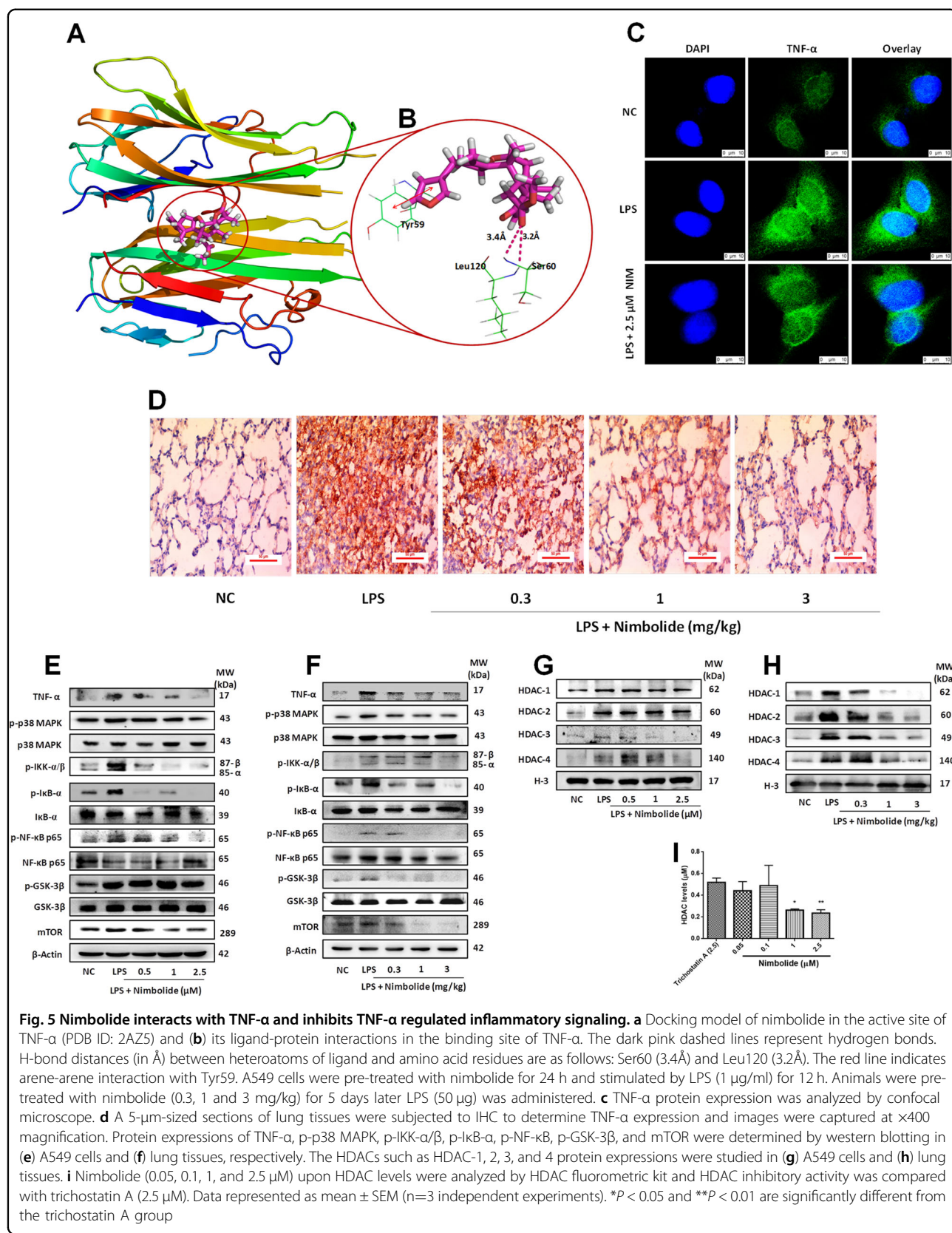


Fig. 5 Nimbolide interacts with TNF-α and inhibits TNF-α regulated inflammatory signaling. **a** Docking model of nimbolide in the active site of TNF-α (PDB ID: 2AZ5) and **(b)** its ligand-protein interactions in the binding site of TNF-α. The dark pink dashed lines represent hydrogen bonds. H-bond distances (in Å) between heteroatoms of ligand and amino acid residues are as follows: Ser60 (3.4 Å) and Leu120 (3.2 Å). The red line indicates arene-arene interaction with Tyr59. A549 cells were pre-treated with nimbolide for 24 h and stimulated by LPS (1 μg/ml) for 12 h. Animals were pre-treated with nimbolide (0.3, 1 and 3 mg/kg) for 5 days later LPS (50 μg) was administered. **c** TNF-α protein expression was analyzed by confocal microscope. **d** A 5-μm-sized sections of lung tissues were subjected to IHC to determine TNF-α expression and images were captured at $\times 400$ magnification. Protein expressions of TNF-α, p-p38 MAPK, p-IKK-α/β, p-IκB-α, p-NF-κB, p-GSK-3β, and mTOR were determined by western blotting in **(e)** A549 cells and **(f)** lung tissues, respectively. The HDACs such as HDAC-1, 2, 3, and 4 protein expressions were studied in **(g)** A549 cells and **(h)** lung tissues. **i** Nimbolide (0.05, 0.1, 1, and 2.5 μM) upon HDAC levels were analyzed by HDAC fluorometric kit and HDAC inhibitory activity was compared with trichostatin A (2.5 μM). Data represented as mean \pm SEM ($n=3$ independent experiments). * $P < 0.05$ and ** $P < 0.01$ are significantly different from the trichostatin A group

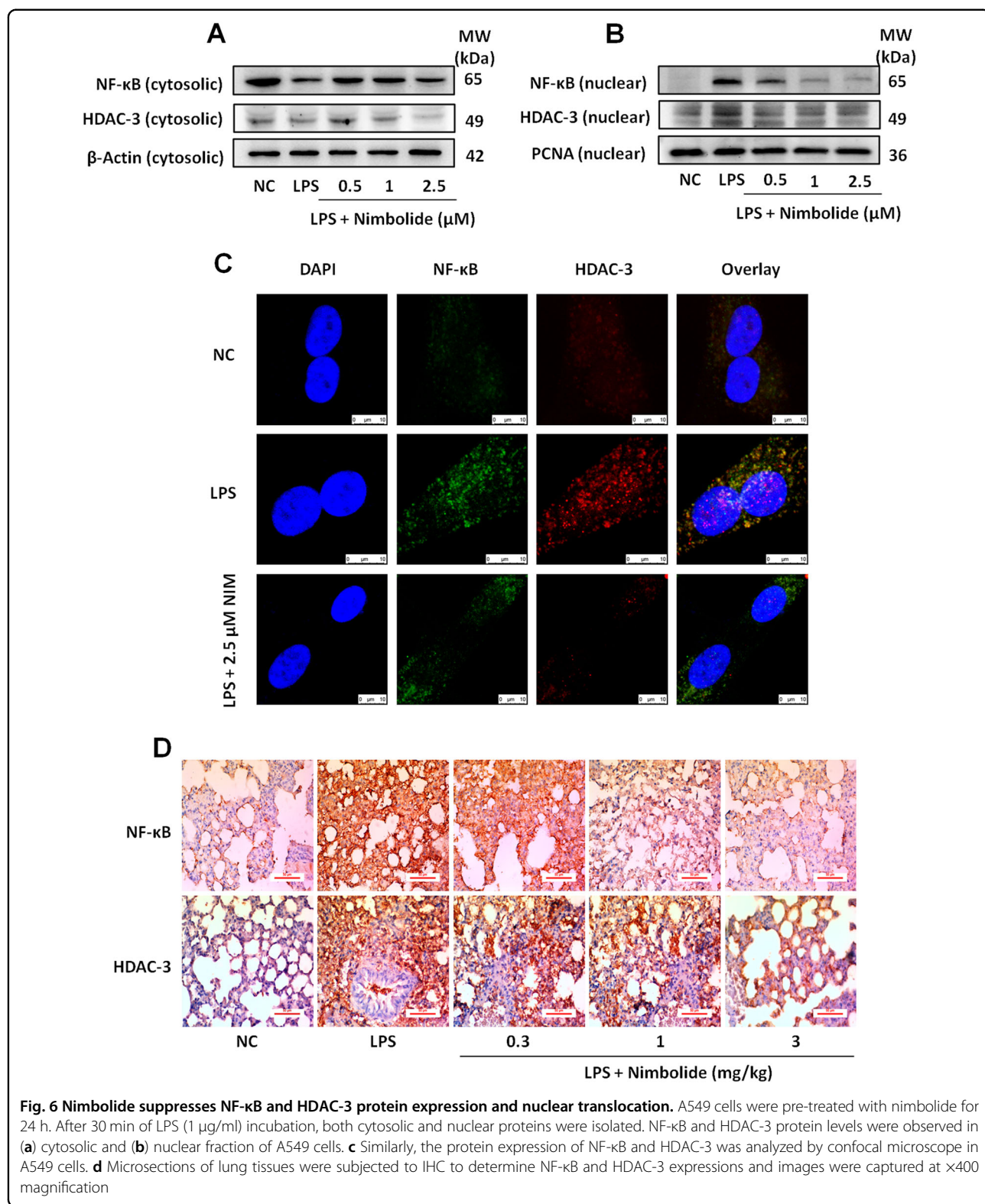
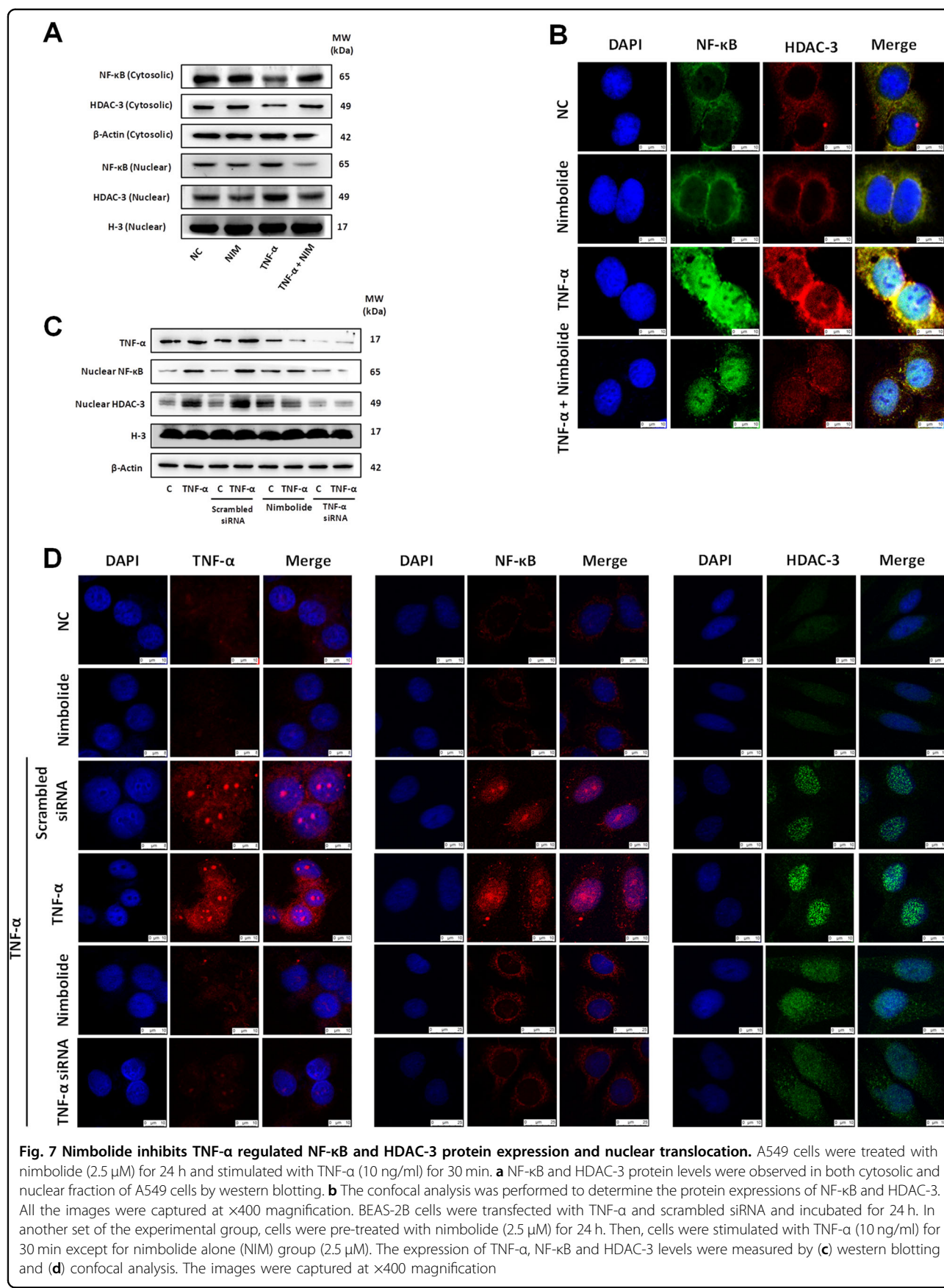


Fig. 6 Nimbulide suppresses NF- κ B and HDAC-3 protein expression and nuclear translocation. A549 cells were pre-treated with nimbulide for 24 h. After 30 min of LPS (1 $\mu\text{g}/\text{ml}$) incubation, both cytosolic and nuclear proteins were isolated. NF- κ B and HDAC-3 protein levels were observed in (a) cytosolic and (b) nuclear fraction of A549 cells. c Similarly, the protein expression of NF- κ B and HDAC-3 was analyzed by confocal microscope in A549 cells. d Microsections of lung tissues were subjected to IHC to determine NF- κ B and HDAC-3 expressions and images were captured at $\times 400$ magnification

immunofluorescence (Fig. 7d). However, the nimbulide alone did not show any significant changes in the expression of TNF- α , nuclear NF- κ B, and HDAC-3 levels

as compared to LPS group and appeared as normal (Supplementary Figure S11). Moreover, the endotoxin-mediated nitrosative stress regulators were unaltered by



nimbolide alone and showed similar results as NC (Supplementary Figure S12).

Discussion

ARDS is a life-threatening condition, which is predominantly associated with a massive number of inflammatory cells migrating to the lung, which could lead to the release of inflammatory mediators that disrupts the alveolar capillary epithelial and endothelial barrier³¹. This loss of integrity increases the permeability and exudates protein-rich serous fluids, which finally leads to lung edema. For this critical anomaly, the corticosteroids would be the preferred choice for treating ARDS patients due to its potent anti-inflammatory and anti-fibrotic activity, but these agents have numerous adverse effects, thus limit the use. To overcome, nowadays, researchers are looking for novel and safer therapeutic approaches for treating ARDS symptoms³². Nimbolide, a natural terpenoid lactone is widely explored in the treatment of various acute and chronic inflammatory diseases³³. As in terms of toxicity, previous reports suggest that nimbolide was found to be toxic upon i.p. administration with LD₅₀ of 225 mg/kg body weight in adult male mice³⁴. In the present study, we have administered much safer doses (0.3, 1, and 3 mg/kg), this sheds the importance of nimbolide in pharmacotherapy. Intriguingly, with the in silico predicted studies, it was observed that nimbolide possess significant physicochemical properties and has the potential to exhibit the properties of drug likeness. The diverse effects of nimbolide and novel insights into its molecular mechanism have been unveiled in the present study.

Enhanced ROS levels activate multiple inflammatory signaling pathways which contribute to pulmonary inflammation. Consistent with literature, we observed an increase in intracellular and mROS levels by LPS in both cultured macrophages and lung tissues. The protective effect of nimbolide was attributed through the decrease in intracellular and mROS production. In accordance, nimbolide modulated a variety of downstream responses that are typically associated with ROS production, apparently through the induction of GSH levels³⁵ and upregulation of Nrf-2, SOD1, and HO-1 expression²⁸. In addition, nimbolide markedly suppressed MPO expression, which is a key regulator of oxidative stress³⁶, thus maintained the redox homeostasis. TNF- α activation by LPS in macrophages induces the mROS levels, thus initiates antimicrobial response³⁷. In our study, we noticed that nimbolide reduced mROS levels with antioxidant activity, without any impairment in bactericidal activity. In turn, an enhanced bactericidal response by macrophages was observed as compared to the control with unknown mechanism. These results were consistent with Hidalgo HA et al., where dexamethasone exhibited TNF- α

inhibitory mechanism, without impairing the macrophage bactericidal activity against Pa²⁶. NO is a well-known nitrosative stress inducer, which is produced by iNOS accompanied by nitrotyrosine and plays a crucial role in ARDS pathology^{38,39}. Here, in our study, we found that nimbolide sequestered the nitrite levels by inhibiting NT and iNOS expression thus, attenuated the exaggerated RNS.

The inflammatory cells such as dendritic cells, macrophages, neutrophils, lymphocytes and eosinophils disrupt the endothelial barrier^{40–42}. Our studies demonstrated that LPS profoundly elevated myriad of inflammatory cells such as total cells, mast cells, WBC, neutrophils, lymphocytes, macrophages, eosinophils, and basophils in BALF⁴³. Strikingly, these initiating aforementioned cytological parameters were reduced markedly with nimbolide treatment. Additionally, LPS induced the platelets and neutrophil count, with concomitantly reduction in Hb levels, whereas nimbolide did not alter these levels.

LPS induced pulmonary inflammation is associated with body temperature alterations like hypothermia, increased lung index due to the inflammatory cell infiltration which could lead to pleural edema²⁰. We observed increased expression of inflammatory cytokines such as IL-1 β , IL-2, IL-6, IL-12 (p40), TNF- α , and TGF- β as well as chemokines MIP-1 α and MIP-1 β in LPS instilled group, further their levels were effectively attenuated by nimbolide treatment. The anti-inflammatory cytokines such as IL-4, IL-10, and IL-13 are expressed by T helper cells 2 and involve in the inhibition of LPS-induced proinflammatory cytokine synthesis⁴⁴. In the present study, nimbolide upregulated the expression of IL-4, IL-10, and IL-13 and preserved the lungs alveolar structure. On the other hand, nimbolide treatment significantly normalized the body weights and exhibited normothermia.

TNF- α has been implicated as a key cytokine in ARDS, which is produced by various cell types including epithelium, endothelium and activated macrophages in response to inflammatory stimuli and considered to be the “master regulator” of proinflammatory cytokines production⁴⁵. TNF- α acts as a central player in initiation and perpetuation of inflammation by orchestrating inflammatory cells activation and recruitment^{46,47}. Hence, pharmacological agents that can either suppress the production of TNF- α or block its biological actions may have potential therapeutic value. Consistently, in the present study, aberrant TNF- α expression was observed in response to LPS stimulation, evidenced at both transcriptional and translational level. It is worthwhile to mention that among the cytokines, a dramatic decline in TNF- α have been observed with nimbolide treatment. On the basis of these results, we speculated that nimbolide executed anti-inflammatory effects through the suppression of TNF- α , which could be the key target. To validate

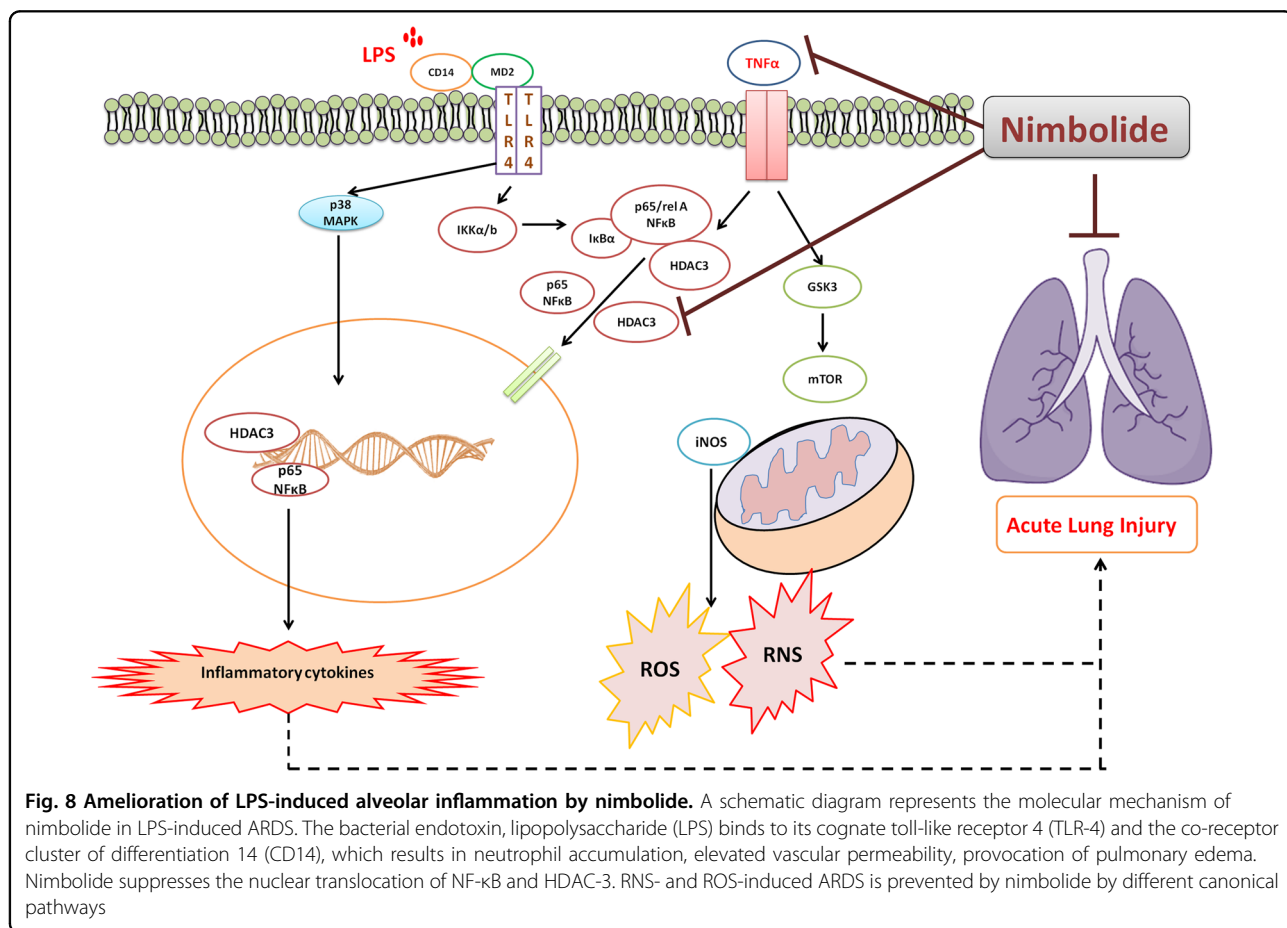
our prediction, we next performed molecular modeling, as hypothesized there was a striking correlation, where we found that nimbolide molecule strongly interacted with TNF- α as compared to its existed co-crystal. Hence, these results prompted us to determine further underlying molecular events associated with TNF- α .

Previous studies have demonstrated a significant role of TNF- α in NF- κ B signaling pathway⁴⁸. Where, IKK- α/β is activated by TNF- α , further it causes phosphorylation of I κ B, which leads to p65 NF- κ B nuclear translocation and induces inflammatory cytokine gene expression⁴⁹. The activation of NF- κ B is critical in mediating in the development of endotoxin-induced ARDS, owing to the worse outcome⁵⁰. Moreover, accumulating evidence suggested that the inflammatory regulator, I κ B- α concomitantly induces HDAC-3 nuclear translocation and further regulates inflammation⁵¹. Intriguingly, H Zhu et al. reported that activation of HDAC-3 and mROS induce the TNF- α expression as a result of crosstalk⁵².

To gain insight into the nimbolide mechanism, epigenetic alterations of HDAC's have been studied. Furthermore, immunoblot results corroborated that LPS stimulation increased HDAC-1, 2, 3, and 4, where nimbolide effectively

reduced the protein expression dose-dependently. These results were consistent with HDAC enzyme assay, where nimbolide inhibited HDAC levels significantly as compared to trichostatin-A. Thus, nimbolide could be the potential emerging molecule as multiple HDAC inhibitor.

In line with the literature, to delineate the crosstalk mechanism, immunoblotting and confocal analysis were performed in A549 cells with LPS/TNF- α stimulation, where we found TNF- α regulated I κ B mediated NF- κ B and HDAC-3 translocation into the nucleus. For more specificity, bronchial epithelial cells were stimulated with TNF- α and observed the consistent mechanism. Interestingly, when we knocked out the TNF- α expression, disappearance of NF- κ B and HDAC-3 was observed in the nucleus. Similarly, nimbolide treatment led to the effective disruption of LPS/TNF- α mediated NF- κ B and HDAC-3 translocation into the nucleus, by inhibiting the phosphorylation of IKK- α/β and I κ B- α , and these results were comparable with specific TNF- α loss of function. Also, we experimentally found that nimbolide remarkably inhibited other TNF- α mediated downstream signaling pathways including, p38 MAPK, GSK-3 β , and mTOR expression.



Our data provided a potential mechanistic link between the TNF- α or LPS induced nuclear translocation of NF- κ B and HDAC-3. A schematic representation of the protection of nimbulide from LPS-induced ARDS inflammatory symptoms is illustrated in Fig. 8. This study emphasized the potential role of nimbulide in inhibiting NF- κ B and HDAC-3 translocation, thereby reducing inflammatory cytokines and maintaining redox balance, thus alleviate the inflammatory symptoms associated with ARDS conditions.

Acknowledgements

We are thankful to the Department of Pharmaceuticals, Ministry of Chemicals and Fertilizers, NIPER-Hyderabad and CSIR-IGIB, New Delhi, India for providing research facilities. Authors would like to thank Dr. Anurag Agrawal, Director of CSIR-IGIB for providing research facilities. The authors also acknowledge Mr. K. Anil Kumar, Research scholar, NIPER-Hyderabad for his technical support during confocal studies. The authors acknowledge Miss. Sheenam Beg, medical student, Government Medical College, Chhattisgarh, India for pathological evaluation.

Author details

¹Department of Regulatory Toxicology, National Institute of Pharmaceutical Education and Research (NIPER), Balanagar, Hyderabad, Telangana 500037, India. ²Centre of Excellence in Asthma & Lung Disease and Molecular Immunogenetics Laboratory, CSIR-Institute of Genomics and Integrative Biology, 110007 New Delhi, India. ³Department of Medicinal Chemistry, National Institute of Pharmaceutical Education and Research (NIPER), Balanagar, Hyderabad, Telangana 500037, India

Author contribution

V.P. designed the experiments, performed the experimental work, analyzed the results and wrote the manuscript. S.T., S.B., B.P. and D.K.S. performed part of the experimental work and/or analyzed the results. N.B.B. and S.B.S. facilitated the manuscript preparation. C.G. conceptualized the study, wrote and revised the manuscript.

Conflict of interest

The authors declare that they have no conflict of interest.

Publisher's note

Springer Nature remains neutral with regard to jurisdictional claims in published maps and institutional affiliations.

Supplementary Information accompanies this paper at (<https://doi.org/10.1038/s41419-018-1247-9>).

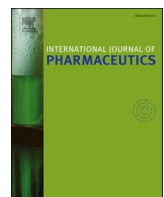
Received: 31 August 2018 Revised: 24 November 2018 Accepted: 27 November 2018

Published online: 28 January 2019

References

- Johnson, E. R. & Matthay, M. A. Acute Lung Injury: epidemiology, pathogenesis, and treatment. *J. Aerosol Med. Pulm. Drug. Deliv.* **23**, 243–252 (2010).
- Rubenfeld, G. D. et al. Incidence and outcomes of acute lung injury. *N. Engl. J. Med.* **353**, 1685–1693 (2005).
- Li, C., Bo, L., Liu, W., Lu, X. & Jin, F. Enteral immunomodulatory diet (omega-3 fatty acid, γ -linolenic acid and antioxidant supplementation) for acute lung injury and acute respiratory distress syndrome: an updated systematic review and meta-analysis. *Nutrients* **7**, 5572–5585 (2015).
- Jeyaseelan, S., Chu, H. W., Young, S. K., Freeman, M. W. & Worthen, G. S. Distinct roles of pattern recognition receptors CD14 and toll-like receptor 4 in acute lung injury. *Infect. Immun.* **73**, 1754–1763 (2005).
- Zanoni, I. et al. CD14 controls the LPS-induced endocytosis of toll-like receptor 4. *Cell* **147**, 868–880 (2011).
- Ramana, K. V. et al. Aldose reductase mediates the lipopolysaccharide-induced release of inflammatory mediators in RAW264.7 murine macrophages. *J. Biol. Chem.* **281**, 33019–33029 (2006).
- Pushpakumar, S. et al. Toll-like receptor 4 deficiency reduces oxidative stress and macrophage mediated inflammation in hypertensive kidney. *Sci. Rep.* **7**, 6349 (2017).
- Mukhopadhyay, S., Hoidal, J. R. & Mukherjee, T. K. Role of TNF α in pulmonary pathophysiology. *Respir. Res.* **7**, 125 (2006).
- Ashburner, B. P., Westerheide, S. D. & Baldwin, A. S. The p65 (RelA) subunit of NF- κ B interacts with the histone deacetylase (HDAC) corepressors HDAC1 and HDAC2 to negatively regulate gene expression. *Mol. Cell. Biol.* **21**, 7065–7077 (2001).
- Gonneaud, A., Gagné, J. M., Turgeon, N. & Asselin, C. The histone deacetylase Hdac1 regulates inflammatory signalling in intestinal epithelial cells. *J. Inflamm. Lond. Engl.* **11**, 43 (2014).
- Ziesché, E. et al. The coactivator role of histone deacetylase 3 in IL-1-signaling involves deacetylation of p65 NF- κ B. *Nucleic Acids Res.* **41**, 90–109 (2013).
- Leus, N. G. J. et al. HDAC 3-selective inhibitor RGFP966 demonstrates anti-inflammatory properties in RAW 264.7 macrophages and mouse precision-cut lung slices by attenuating NF- κ B p65 transcriptional activity. *Biochem. Pharmacol.* **108**, 58–74 (2016).
- Usui, T. et al. HDAC4 mediates development of hypertension via vascular inflammation in spontaneous hypertensive rats. *Am. J. Physiol. Heart Circ. Physiol.* **302**, H1894–H1904 (2012).
- Dong, W. et al. Sodium butyrate activates NRF2 to ameliorate diabetic nephropathy possibly via inhibition of HDAC. *J. Endocrinol.* **232**, 71–83 (2017).
- Leus, N. G. J. et al. HDAC1-3 inhibitor MS-275 enhances IL10 expression in RAW264.7 macrophages and reduces cigarette smoke-induced airway inflammation in mice. *Sci. Rep.* **7**, 45047 (2017).
- Pooladanda, V., Bandi, S., Mondi, S. R., Gottumukkala, K. M. & Godugu, C. Nimbulide epigenetically regulates autophagy and apoptosis in breast cancer. *Toxicol. Vitr.* **51**, 114–128 (2018).
- Nekkanti, S. et al. Synthesis of 1,2,3-triazolo-fused-tetrahydro- β -carboline derivatives via 1,3-dipolar cycloaddition reaction: cytotoxicity evaluation and DNA-binding studies. *ChemistrySelect* **2**, 7210–7221 (2017).
- Jain, A. et al. Liposphere mediated topical delivery of thymoquinone in the treatment of psoriasis. *Nanomed. Nanotechnol. Biol. Med.* **13**, 2251–2262 (2017).
- Rahman, I., Kode, A. & Biswas, S. K. Assay for quantitative determination of glutathione and glutathione disulfide levels using enzymatic recycling method. *Nat. Protoc.* **1**, 3159–3165 (2006).
- Card, J. W. et al. Gender differences in murine airway responsiveness and lipopolysaccharide-induced inflammation. *J. Immunol.* **177**, 621–630 (2006).
- Pohl, C. S. et al. Early weaning stress induces chronic functional diarrhea, intestinal barrier defects, and increased mast cell activity in a porcine model of early life adversity. *Neurogastroenterol. Motil.* **29**, e13118 (2017).
- Godugu, C. et al. Inhalation delivery of telmisartan enhances intratumoral distribution of nanoparticles in lung cancer models. *J. Control. Release* **172**, 86–95 (2013).
- Godugu, C., Patel, A. R., Doddapaneni, R., Somagoni, J. & Singh, M. Approaches to improve the oral bioavailability and effects of novel anticancer drugs berberine and betulinic acid. *PLoS ONE* **9**, e89919 (2014).
- Kaur, J. & Tikoo, K. p300/CBP dependent hyperacetylation of histone potentiates anticancer activity of gefitinib nanoparticles. *Biochim. Biophys. Acta* **1833**, 1028–1040 (2013).
- He, M. M. et al. Small-molecule inhibition of TNF-alpha. *Science* **310**, 1022–1025 (2005).
- Hidalgo, H. A., Helmke, R. J., German, V. F. & Mangos, J. A. The effects of cyclosporine and dexamethasone on an alveolar macrophage cell line (NR8383). *Transplantation* **53**, 620–623 (1992).
- Speyer, C. L. et al. Regulatory effects of iNOS on acute lung inflammatory responses in Mice. *Am. J. Pathol.* **163**, 2319–2328 (2003).
- Ma, Q. Role of Nrf2 in oxidative stress and toxicity. *Annu. Rev. Pharmacol. Toxicol.* **53**, 401–426 (2013).
- Whitehead, G. S. et al. TNF is required for TLR ligand-mediated but not protease-mediated allergic airway inflammation. *J. Clin. Invest.* **127**, 3313–3326 (2017).
- Cross, L. J. M. & Matthay, M. A. Biomarkers in acute lung injury: insights into the pathogenesis of acute lung injury. *Crit. Care Clin.* **27**, 355–377 (2011).

31. Wilson, K. C. & Saukkonen, J. J. Acute respiratory failure from abused substances. *J. Intensive Care. Med.* **19**, 183–193 (2004).
32. Reutershaw, J. & Ley, K. Bench-to-bedside review: acute respiratory distress syndrome – how neutrophils migrate into the lung. *Crit. Care.* **8**, 453–461 (2004).
33. Wang, L. et al. Anticancer properties of nimbolide and pharmacokinetic considerations to accelerate its development. *Oncotarget* **7**, 44790–44802 (2016).
34. Glinsukon, T., Somjaree, R., Piyachaturawat, P. & Thebtaranonth, Y. Acute toxicity of nimbolide and nimbic acid in mice, rats and hamsters. *Toxicol. Lett.* **30**, 159–166 (1986).
35. Kerkick, C. & Willoughby, D. The Antioxidant role of glutathione and N-acetylcysteine supplements and exercise-induced oxidative stress. *J. Int. Soc. Sports Nutr.* **2**, 38–44 (2005).
36. Anatoliotakis, N. et al. Myeloperoxidase: expressing inflammation and oxidative stress in cardiovascular disease. *Curr. Top. Med. Chem.* **13**, 115–138 (2013).
37. West, A. P. et al. TLR signaling augments macrophage bactericidal activity through mitochondrial ROS. *Nature* **472**, 476–480 (2011).
38. Hanafy, K. A., Krumenacker, J. S. & Murad, F. NO, nitrotyrosine, and cyclic GMP in signal transduction. *Med. Sci. Monit.* **7**, 801–819 (2001).
39. Korhonen, R., Lahti, A., Kankaanranta, H. & Moilanen, E. Nitric oxide production and signaling in inflammation. *Curr. Drug. Targets Inflamm. Allergy* **4**, 471–479 (2005).
40. Grommes, J. & Soehnlein, O. Contribution of neutrophils to acute lung injury. *Mol. Med.* **17**, 293–307 (2011).
41. Kato, A., Hulse, K. E., Tan, B. K. & Schleimer, R. P. B-lymphocyte lineage cells and the respiratory system. *J. Allergy Clin. Immunol.* **131**, 933–957 (2013).
42. Moldoveanu, B. et al. Inflammatory mechanisms in the lung. *J. Inflamm. Res.* **2**, 1–11 (2009).
43. Nakagome, K. & Nagata, M. Pathogenesis of airway inflammation in bronchial asthma. *Auris Nasus Larynx* **38**, 555–563 (2011).
44. Bryant, A. H., Spencer-Harty, S., Owens, S. E., Jones, R. H. & Thornton, C. A. Interleukin 4 and interleukin 13 downregulate the lipopolysaccharide-mediated inflammatory response by human gestation-associated tissues. *Biol. Reprod.* **96**, 576–586 (2017).
45. Lundblad, L. K. A. et al. Tumor necrosis factor- α overexpression in lung disease. *Am. J. Respir. Crit. Care. Med.* **171**, 1363–1370 (2005).
46. Parameswaran, N. & Patial, S. Tumor necrosis factor- α signaling in macrophages. *Crit. Rev. Eukaryot. Gene Expr.* **20**, 87–103 (2010).
47. Liu, Z. et al. Inhibitory effects of rosiglitazone on paraquat-induced acute lung injury in rats. *Acta Pharmacol. Sin.* **34**, 1317–1324 (2013).
48. Shi, L., Kishore, R., McMullen, M. R. & Nagy, L. E. Lipopolysaccharide stimulation of ERK1/2 increases TNF-alpha production via Egr-1. *Am. J. Physiol. Cell. Physiol.* **282**, C1205–C1211 (2002).
49. Zidi, I., Mestiri, S., Bartegi, A. & Amor, N. B. TNF-alpha and its inhibitors in cancer. *Med. Oncol.* **27**, 185–198 (2010).
50. Li, Y. et al. Angiotensin-converting enzyme 2 prevents lipopolysaccharide-induced rat acute lung injury via suppressing the ERK1/2 and NF- κ B signaling pathways. *Sci. Rep.* **6**, 27911 (2016).
51. Gao, Z., He, Q., Peng, B., Chiao, P. J. & Ye, J. Regulation of nuclear translocation of HDAC3 by IkappaBalpha is required for tumor necrosis factor inhibition of peroxisome proliferator-activated receptor gamma function. *J. Biol. Chem.* **281**, 4540–4547 (2006).
52. Zhu, H., Shan, L., Schiller, P. W., Mai, A. & Peng, T. Histone deacetylase-3 activation promotes tumor necrosis factor- α (TNF- α) expression in cardiomyocytes during lipopolysaccharide Stimulation. *J. Biol. Chem.* **285**, 9429–9436 (2010).



BRD4 targeting nanotherapy prevents lipopolysaccharide induced acute respiratory distress syndrome

Venkatesh Pooladanda, Sowjanya Thatikonda, Sai Priya Muvvala, Geetanjali Devabattula, Chandraiah Godugu*

Department of Regulatory Toxicology, National Institute of Pharmaceutical Education and Research (NIPER), Balanagar, Hyderabad, Telangana 500037, India

ARTICLE INFO

Keywords:
ARDS
BRD4
Lipoplexes
Cytokine storm
p65
STAT3 nuclear translocation

ABSTRACT

Acute respiratory distress syndrome (ARDS) is a life threatening respiratory disease associated with pulmonary edema, alveolar dysfunction, hypoxia, and inflammatory cell accumulation. The most contagious form of COVID-19 associated with ARDS caused by SARS-CoV-2. SARS-CoV-2 majorly produces the cytokine storm and severe lung inflammation and ultimately leads to respiratory failure. ARDS is a complex disease and there is no proper therapeutics for effective therapy. Still, there is a huge scope to identify novel targets to combat respiratory illness. In the current study, we have identified the epigenetic regulating protein BRD4 and developed siRNA based nanomedicine to treat the ARDS. The liposomes were prepared by thin-film hydration method, where BRD4 siRNA complexed with cationic lipid and exhibited 96.24 ± 18.01 nm size and stable even in the presence of RNase. BRD4 siRNA lipoplexes (BRD4-siRNA-LP) inhibited inflammatory cells in lungs and suppressed the lipopolysaccharide (LPS) induced the neutrophil infiltration and mast cell accumulation. Also, BRD4 siRNA based nanomedicine significantly reduced the LPS induced cytokine storm followed by inflammatory signaling pathways. Interestingly, BRD4-siRNA-LP suppressed the LPS-induced p65 and STAT3 nuclear translocation and ameliorated the lung inflammation. Thus, BRD4-siRNA-LP could be a plausible therapeutic option for treating ARDS and might be useful for combating the COVID-19 associated respiratory illness.

1. Introduction

Acute respiratory distress syndrome (ARDS) is the pathological condition in critically ill patients associated with pulmonary infiltration and emphysema. ARDS is caused by various etiological factors such as inhalation of toxicants, trauma, adverse drug reactions, drug over-dosage, sepsis, and pancreatitis that accounts for 35–46% mortality (Bellani et al., 2016; Diamond et al., 2020). Recently, the Coronavirus Disease 2019 (COVID-19 Map, n.d) represents respiratory illness from Severe Acute Respiratory Syndrome Coronavirus 2 (SARS-CoV-2) infection, and became a potential pandemic with more than 132,662,731 sufferers and around 2,877,835 deaths all over the world (Worldometer, 2021). ARDS is one of the main complications in COVID-19 patients that causes diffuse alveolar damage in the lungs in 42% of patients and 61–81% of that requiring intensive care unit (ICU) support. The COVID-19 induced ARDS is showing wreaking havoc in countries such as the USA, Brazil, India, Russia, UK, Spain, and Italy while ARDS patients have been sustaining in ICU under the ventilation. This virus-

associated severe ARDS has a poor prognosis with no proper treatment and various researchers are working on repurposing drugs for symptomatic relief (Möhlenkamp and Thiele, 2020).

LPS (Lipopolysaccharide) is a bacterial endotoxin present on the outer membrane of gram-negative bacteria, an agonist for Toll-like receptor 4 (TLR-4) that mimics the sepsis induced ARDS both *in vitro* and *in vivo* (Pu and Wang, 2014). LPS stimulates macrophages, mast cells, and neutrophils and produces pneumonia-related severe respiratory distress syndrome ultimately causing respiratory failure (Xu and Shi, 2012). Macrophages are large phagocytic cells found in tissues and blood and mainly appear predominantly in inflammatory conditions (Fujiwara and Kobayashi, 2005). Additionally, LPS induces oxidative stress and further induce pulmonary edema and impairs pulmonary endothelial barrier function, which is the characteristic phenomenon of the severe acute respiratory syndrome (Grinnell et al., 2012). LPS stimulation enhances the proinflammatory cytokine levels by activating the p65 nuclear factor kappa-light-chain-enhancer of activated B cells (NF-κB), Protein kinase B (Akt), mitogen-activated protein kinase (MAPK) signaling pathways

* Corresponding author.

E-mail address: chandraiah@niperhyd.ac.in (C. Godugu).

which are involved in the perpetuation of the inflammatory responses (Alvira, 2014; Guha and Mackman, 2002; Selvaraj et al., 2015). LPS stimulation also triggers the translocation of transcription factors p65 NF- κ B as well as Signal transducer and activator of transcription 3 (STAT3) from cytoplasm to nucleus, thus initiates the transcription of various proinflammatory genes responsible for cytokine storm (Bagaev et al., 2019). LPS induced inflammation may mimic the sepsis condition and most of the aspects of COVID-19 associated ARDS, although, it does not completely resemble the SARS-CoV-2 induced ARDS, but the deleterious effects associated can be resembled. The bromodomain (BD) is a structural motif within the proteins family that recognizes the acetylated lysine residues and employed in epigenetic modification through histone regulation as “readers” that orchestrate gene transcription (Miller et al., 2016). The bromodomain and extra terminal domain (BET) proteins are identified as BRD2, BRD3, BRD4, and testis-specific BRDT, among all, BRD4 plays an important role in inflammation and cancer (Klein, 2018). Generally, BET proteins have two conserved BDs, they involve recognizing acetylated histones and act as scaffolds to recruit transcriptional co-activators to promoters and super-enhancers, thereby drive gene transcription (Cochran et al., 2019). In inflammation, BDs identify the acetylated lysines on non-histone proteins such as RelA known as p65 NF- κ B, which plays an important role in this condition (Hajmirza et al., 2018). BRD4 inhibitors were used in alleviating various diseases in the lung inflammation, cancer etc., and most of these are under clinical trials (Duan et al., 2018). However, BRD4 mechanism and its role in ARDS condition are not clear. Hence, in the current study, we evaluated the role of BRD4 in mediating inflammatory responses. Furthermore, BRD4 was attenuated with siRNA to abrogate its function and the effect was investigated.

Lipoplexes are the cationic liposomes, classically used as nonviral synthetic lipid carriers of DNA. These lipoplexes enhance the therapeutic bioavailability of drugs or genes through enhanced permeability and retention (EPR) effect (Deshpande et al., 2013). These lipoplexes are widely used in gene delivery including small interfering RNA (siRNA), micro RNA (miRNA), and short hairpin RNA (shRNA) (Shim et al., 2013). siRNAs are artificially synthesized 20–30 nucleotides long double-stranded RNA molecules, which are routinely used in molecular biology for transient silencing of a gene of interest. They elicit RNA interference (RNAi) response upon binding to their target transcript based on the sequence complementarity and siRNA therapeutics are employed as an alternative to traditional drugs for the management of various diseases (Dana et al., 2017). However, safe and effective siRNA delivery to the affected site is hampered by poor stability, highly hydrophilic nature, and low cellular uptake of siRNA (Wang et al., 2010). siRNA is negative in charge and forms the electrostatic interactions with cationic lipid DOTAP and forms lipoplexes. Further, these siRNA lipoplexes were taken up by cells through endocytosis mediated pathway (Alshehri et al., 2018; Schroeder et al., 2010). Mainly, in lung diseases, siRNA lipoplexes are administered to lungs through inhalation or intravenous route, as this route of administration of siRNA lipoplexes have the advantage of being less invasive (Qiu et al., 2016). In the current study, for delivering the BRD4 siRNA into the lungs, we have prepared the nanosized cationic lipoplexes for the downregulation of corresponding BRD4 mRNA and further investigated the mechanistic insights of BRD4 inhibition in LPS induced ARDS conditions both *in vitro* and *in vivo*.

2. Materials and methods

2.1. Chemicals

BRD4 siRNA was procured from Santa Cruz Biotechnology, USA. 1,2-dioleoyl-3-trimethyl ammonium propane (DOTAP) (chloride salt) was purchased from Avanti polar lipids, USA. LPS from Escherichia coli (055:B5), PFI-1, Cholesterol (Chol), Trizma Base, SDS, acrylamide, DCFDA, and FITC were procured from Sigma Aldrich, USA. Agarose was

procured from Merck, USA. SYBR Green I was purchased from Thermo Fisher Scientific, USA. The primary and secondary antibodies were purchased from Cell Signaling Technologies, USA and Santa Cruz Biotechnology, USA, respectively. All the chemicals which are used in this study are analytically pure and molecular grade.

2.2. Preparation of BRD4 siRNA DOTAP lipoplexes

BRD4 siRNA lipoplexes (BRD4-siRNA-LP) were prepared using the previously reported methods by dissolving DOTAP and Chol in chloroform in a 1:1 M ratio (Pandi et al., 2018). Thin-film was formed by rotary evaporation, which is hydrated with Diethylpyrocarbonate (DEPC) treated water at 37 °C to form multilamellar vesicles (MLV). Further, MLV containing liposomes were subjected to probe sonication to form nanosized liposomes. The stable complex of siRNA lipoplexes was prepared by mixing the siRNA/lipid (N/P) molar ratio by incubating at 37 °C for 30 min. Whereas, blank lipoplexes (Blank-LP) were prepared similar to siRNA lipoplexes without BRD4 siRNA.

2.3. Gel retardation and integrity assay

siRNA easily undergoes ribonucleolytic degradation, while the lipoplex form enhances the stability, agarose gel electrophoresis is used to study the formation of BRD4-siRNA-LP (Patil et al., 2011). In this study, to test the stability of BRD4 siRNA in lipoplexes, they were prepared and loaded on to the gel by mixing in 1X loading dye. Plain BRD4 siRNA was employed for comparison. 3% agarose gel was prepared by adding ethidium bromide and electrophoresis was performed under the conditions of 60 mA for 35 min. The bands were visualized by the Chemidoc system at 365 nm.

2.4. Determination of particle size and entrapment efficiency

Lipoplexes particle size and size distribution were measured by Zetasizer Nano-ZS in DTS0012 plastic cells (Malvern instrument Ltd. UK). The entrapment of siRNA in cationic lipoplexes was determined as described earlier (Jain et al., 2017), where the standard curve of siRNA was plotted by using the nanodrop spectrophotometer and calculated the unknown concentration of siRNA in the supernatant after centrifugation of lipoplexes at 16000 rpm for 10 min from the standard curve followed by measured the bounded and unbounded siRNA concentration from the values. The percentage of entrapment efficiency was calculated using the following formula.

$$\% \text{ Entrapment efficiency} = \frac{\text{Encapsulated siRNA concentration}}{\text{Initial siRNA concentration}} \times 100$$

2.5. Cell culture

Mouse macrophages (RAW 264.7 cells) were procured from National Center for Cell Sciences (NCCS), Pune, India. Cells were grown in 10% FBS supplemented 1% Antibiotic and anti-mycotic solution containing DMEM high glucose medium by incubating in a humidified CO₂ incubator at 37°C temperature. Cells were trypsinized and sub-cultured when they attained 80% confluence.

2.6. DCFDA staining

RAW 264.7 cells were pretreated with 10 nM of BRD4-siRNA-LP for 48 h and stimulated with LPS for 30 min. Later cells were stained with 10 μM concentration of DCFDA and incubated for 15 min. Images were captured at $\times 200$ magnification using fluorescent microscopy.

2.7. Animals

6–8 weeks old male C57/BL6 mice (weight 25–30 g) were purchased

from Palamur Biosciences, Mahabubnagar, India. Animals were housed in specific pathogen-free conditions with 12 h day/night cycle. All animals were acclimatized at least one week prior to initiating the experiment. All procedures of the study were approved by the Institutional Animal Ethics Committee (IAEC), NIPER-Hyderabad, India. All the experiments were conducted following the Committee for the Purpose of Control and Supervision of Experiments on Animals (CPCSEA) guidelines, the government of India.

2.8. ARDS model development and treatment

In *in vivo*, mice were divided into 7 groups ($n = 8$) including normal control (NC), LPS control, BRD4-siRNA-LP control, blank lipoplexes (Blank-LP), BRD4-siRNA-LP pretreatment (Pre) and concurrent (Con) treatment and PFI-1 (5 mg/kg) groups. In the pretreatment group, animals were administered with BRD4-siRNA-LP 5 days before LPS stimulation, where the concurrent group animals received BRD4-siRNA-LP along with LPS. Here, mice were treated with 500 nM siRNA. Whereas, NC group animals received only PBS. Here, the lipoplexes, PFI-1, LPS, and PBS were administered by the oropharyngeal route. Animals were sacrificed by isoflurane overexposure after 12 h of LPS post-stimulation. The collected lung tissues were stored in -80°C .

2.9. Physiological parameters

Net body weight changes measured by taking the values before and after LPS stimulation and lung weight index was calculated as described earlier (Pooladanda et al., 2019).

2.10. Bronchoalveolar lavage (BAL) fluid analysis

After sacrifice, lungs were lavaged with ice-cold PBS for 3 times, bronchoalveolar samples were collected, pooled, and centrifuged for 10 min at $300 \times g$. Cell pellets obtained were suspended in PBS (1 ml) and subjected to differential cell counter ADVIA 2120i hematology system (Siemens, Germany).

2.11. Enzyme-linked immunosorbent assay (ELISA)

IL-1 β , IL-6, IL-17A, IL-22, and TNF- α levels in lung tissue lysates were analyzed by ELISA according to the manufacturer instructions (Thermo Fisher Scientific, USA).

2.12. Immunofluorescence

Specific Antigen-antibody interaction, location, and distribution can be determined by immunofluorescence by using the fluorochrome detection system. In this method, cells were fixed in 4% paraformaldehyde and permeabilized with 0.1% Triton X-100, whereas 5 μm sections of lung tissues were deparaffinized, rehydrated and then antigen was unmasked by treating with proteinase k for 15 min. Non-specific binding portions were eliminated by 3% BSA blocking solution and incubated with primary antibodies (1:100 dilutions) overnight at 4°C and later suitable dye conjugated secondary antibodies were added and incubated. Cells and tissue sections were washed thrice with immune wash buffer and probed with rhodamine or fluorescein isothiocyanate (FITC) (Sigma-Aldrich, USA) conjugated anti-mouse or anti-rabbit (1:200 dilutions) for 1 h and nuclei was stained with DAPI stain (Sigma-Aldrich, USA), after mounting slides with Fluoreshield™ histology medium, visualized under the confocal microscope.

2.13. Haematoxylin and eosin (H&E) staining

Lung tissues were moulded in paraffin wax, and tissue sectioning was performed by microtome (Leica, Germany). Poly-L-Lysine coated slides were used to collect the tissue sections. For histological evaluation,

tissue sections were stained with H&E and visualized under the microscope at $\times 400$ magnification Histopathological score was determined as described earlier (Pooladanda et al., 2021).

2.14. Toluidine blue staining

Tissue sections were stained with toluidine blue (TB) and evaluated the mast cell infiltration. Images were captured at $\times 400$ magnifications by bright-field microscope (Olympus CX21i, Japan). Mast cells were counted and represented as described earlier (Pooladanda et al., 2019).

2.15. Western blotting

Protein lysate was extracted from cells as well as from lung tissues as described earlier (Thatikonda et al., 2020). Bicinchoninic acid (BCA) calorimetric assay kit (Sigma-Aldrich, USA) was used for the estimation of protein concentration. Protein samples were loaded and subjected to Sodium dodecyl sulfate-Polyacrylamide gel electrophoresis (SDS-PAGE). Proteins were electrotransferred according to their molecular weight onto nylon membrane (Sigma-Aldrich, USA); later proteins were visualized based on their molecular weights by placing membranes in Ponceau S stain. Non-specific binding of antibodies was avoided by a 3% blocking solution and incubated overnight with primary antibody at 4°C , later secondary antibody was added and detected by using enhanced chemiluminescence (ECL) substrate (Bio-Rad, USA). Blots were developed by the Chemidoc imaging system (Vilber Fusion Fx, France). Images were analyzed by ImageJ software, NIH, USA. Protein normalization was done by β -Actin and their respective total proteins.

2.16. Statistical analysis

All the results were analyzed by Graphpad Prism, USA (version 6.01) software, where n represents the number of replicates. One-way analysis of variance (ANOVA) was applied along with the Bonferroni post hoc test for statistical analysis. Here, $p < 0.05$ was considered statistically significant.

3. Results

3.1. Characterization of BRD4-siRNA-LP

Lipoplexes were prepared by thin-film hydration method. The particle size, polydispersity index (PDI), and charge were determined by Zetameter. Where, the particle size of Blank-LP and BRD4-siRNA-LP were found to be 95.25 ± 9.49 (Fig. 1A) and 96.24 ± 18.01 nm (Fig. 1B), respectively, whereas the PDI was found to be 0.24 ± 0.02 and 0.25 ± 0.03 , respectively. The Blank-LP and BRD4-siRNA-LP exhibited charge of 32.78 ± 2.71 (Fig. 1C) and 30.25 ± 2.01 mV (Fig. 1D), respectively. Stable complexes are a prerequisite to deliver the siRNA and to overcome serum instability or a high clearance rate *in vivo* (Pal Singh et al., 2020). We first analyzed the integrity of BRD4 siRNA and gel retardation by agarose gel electrophoresis. Equimolar concentrations of BRD4-siRNA were complexed with different molar ratios of cationic lipoplexes. The assay results reveal that with gradual increase in the lipoplexes concentrations 1:10, 1:50, 1:100 and 1:200 ratio with equimolar concentration of BRD4-siRNA, there was enhanced resistance towards serum nuclease with preserved RNAi activity at 1:200 with significant stable ionic interactions as compared to other concentrations. While the naked siRNA was found to be degraded in the presence of nuclease (Fig. 1E). Further, we chose 1:200 ratio stable complex of BRD4-siRNA-LP for performing all the biological and molecular studies. The entrapment efficiency that determines the amount of siRNA present in prepared lipoplexes was evaluated by nanodrop method. The entrapment efficiency of BRD4-siRNA-LP (1:200) was found to be $85.65 \pm 0.98\%$, and also shows enhanced stability of BRD4-siRNA-LP, whereas plain BRD4 siRNA was easily degraded in presence of RNase (Fig. 1F).

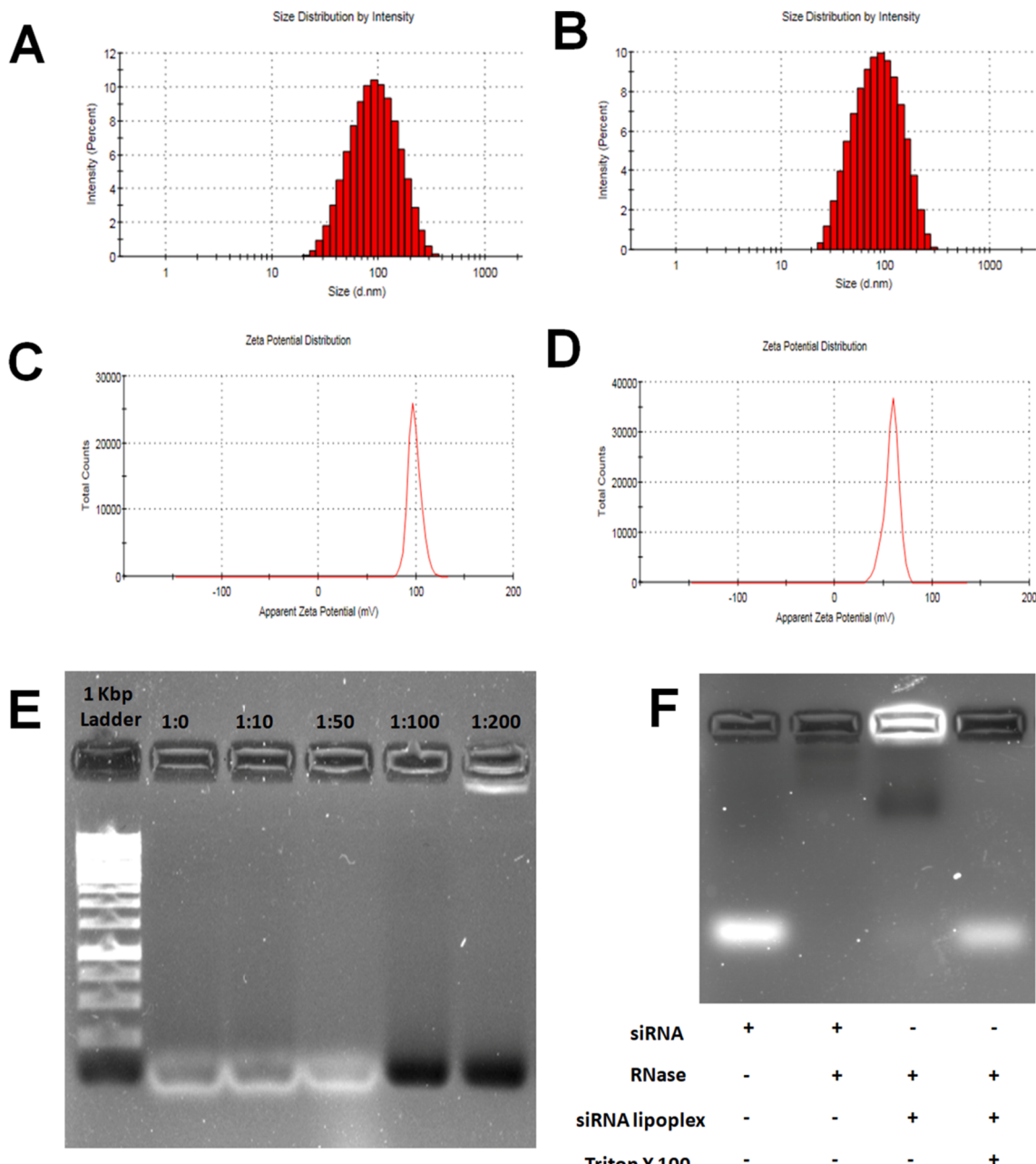


Fig. 1. BRD4-siRNA-LP particles size and charge characterization. The cationic lipoplexes were prepared by thin-film hydration method by taking an equal ratio of DOTAP and Chol. The particle size of (A) Blank-LP and (B) BRD4-siRNA-LP as well as potential of (C) Blank-LP and (D) BRD4-siRNA-LP were determined by Zetasizer. (E) Gel retardation and integrity assay and (F) RNase protection assay were performed by agarose electrophoresis using different molar ratios of BRD4 siRNA and cationic lipoplexes.

Collectively, the prepared BRD4-siRNA-LP were nanosized, exhibited uniform size with positive charge and formed stable complexes.

3.2. BRD4-siRNA-LP modulate physiological changes and control the proinflammatory cells by targeting BRD4 in LPS induced ARDS mouse model

Western blot results revealed that BRD4-siRNA-LP significantly suppressed LPS induced BRD4 expression in lung tissues, similar kind of decreased expression was also observed with BRD4 inhibitor PFI-1 (Fig. 2A and Figure S1A). The oropharyngeal administration of LPS in mice led to a decrease in net body weight (Fig. 2B), and significantly increased the lung weight index (Fig. 2C), which further contributes to pulmonary edema. Interestingly, oropharyngeal administration of

BRD4-siRNA-LP showed prominent results in modulating LPS induced physiological changes. Both BRD4-siRNA-LP pretreatment and concurrent treatment groups showed satisfactory results as compared to small molecule inhibitor PFI-1. However, in Blank-LP group, there were no significant LPS induced changes were observed. Whereas, BRD4-siRNA-LP alone group exhibited no apparent changes and appeared to be similar to normal control (NC). Targeting BRD4 and its inhibition significantly reduced the endothelial barrier dysfunction followed by suppression of alveolar disruption. The inflammatory responsive cells, including total BAL cells (Fig. 2D), white blood cells (WBC) (Fig. 2E), neutrophils (Fig. 2F), basophils (Fig. 2G), and macrophages (Fig. 2H) were upregulated in LPS treated animals. Whereas BRD4-siRNA-LP treatment including pre-treatment and concurrent groups exhibited decreased inflammatory cell number as compared to LPS stimulated

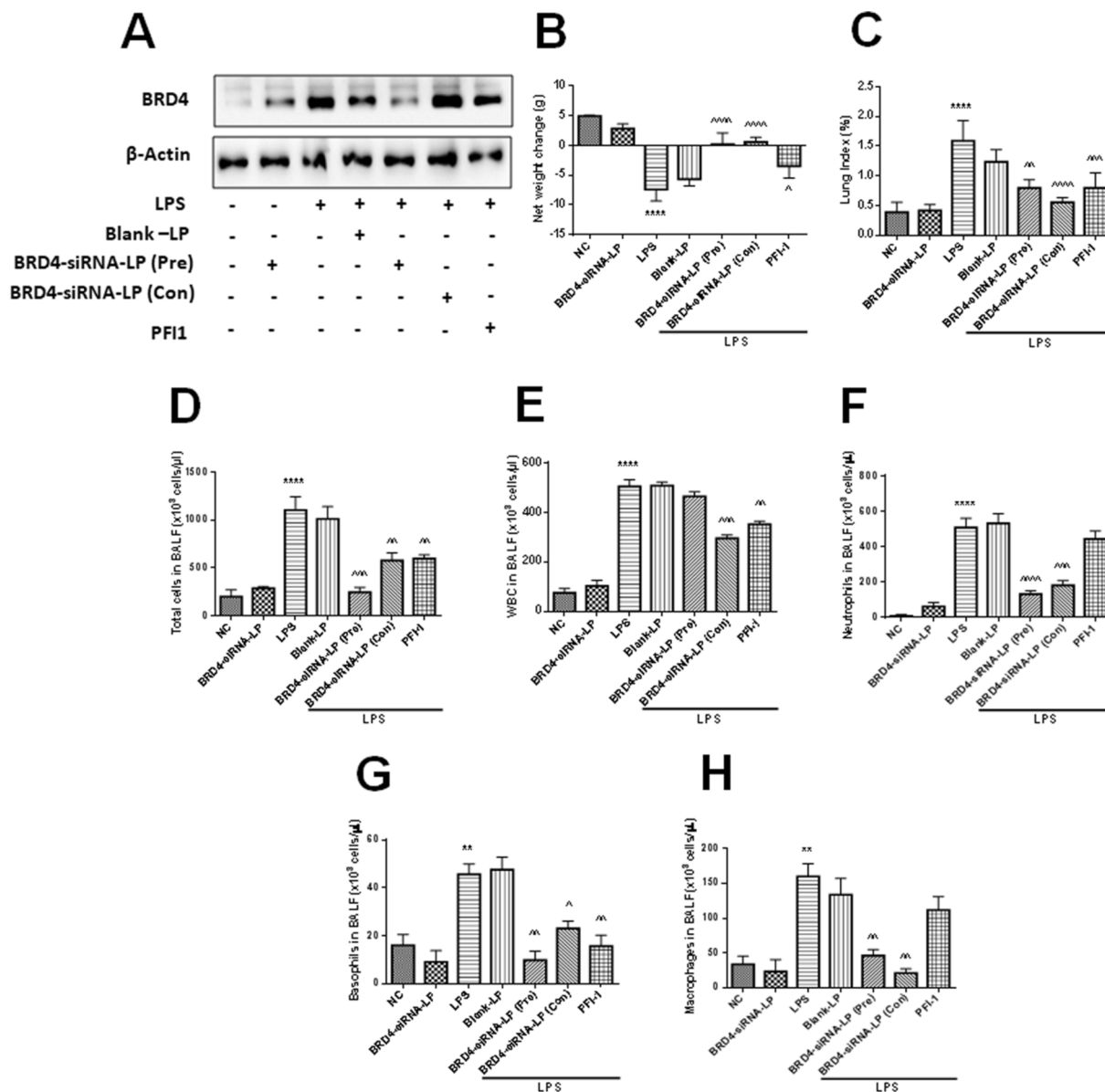


Fig. 2. BRD4-siRNA-LP inhibit LPS induced physiological changes and suppress inflammatory responsive cells in BALF. BRD4-siRNA-LP (500 nM/mouse) were administered through oropharyngeal route at 5 days pre-treatment and concomitant modes, and the effect on LPS induced (A) BRD4 expression, physiological changes such as (B) net body weight changes and (C) lung weight indexes were observed in C57/BL6 mice model. BALF was aspirated with chilled PBS and subjected to differential blood cell counter for estimating the count of inflammatory responsive cells include (D) total cells, (E) WBC, (F) neutrophils, (G) basophils, and (H) macrophages. Data presented as mean \pm SD (n = 8 animals per group). **P < 0.01 and ****P < 0.0001 are significantly different from the NC group; ^P < 0.05, ^P < 0.01, ^~P < 0.001, and ^~~P < 0.0001 are significantly different from the LPS group. Here, Blank-LP = Blank Lipoplexes; BRD4-siRNA-LP = BRD4 siRNA Lipoplexes; BRD4-siRNA-LP (Pre) = BRD4 siRNA Lipoplexes pretreatment; BRD4-siRNA-LP (Con) = BRD4 siRNA Lipoplexes concurrent treatment.

group animals. Here, we observed that as compared to PFI-1 treated group, BRD4-siRNA-LP treatment showed superior effects, whereas BRD4-siRNA-LP alone group exhibited safer profiles with the results similar to NC group. Thus, targeting BRD4 with lipoplexes reduced pulmonary edema and cell-mediated inflammation.

3.3. BRD4-siRNA-LP inhibit nitrosative stress and pro-inflammatory cytokine levels in ARDS mouse model

Nitrosative and oxidative stress play an important role in inducing alveolar disruption and irreversible damage to critical biomolecules such as lipids, proteins and DNA further responsible for respiratory collapse (Thimmulappa et al., 2019). The TLR4 agonist LPS induces respiratory illness by exacerbating the oxidative stress non-selectively, with accompanying nitrosative stress (Soodaeva et al., 2019). Both

pre-treatment and concurrent BRD4-siRNA-LP treated groups showed reduced nitrite levels as compared to LPS control group. The treatment groups which include PFI-1, concurrent BRD4-siRNA-LP group showed a prominent reduction in nitrite levels, whereas the BRD4-siRNA-LP alone group exhibited no significant changes in healthy animals (Fig. 3A). Nitrosative and oxidative stress were neutralized by anti-oxidant defensive switches that include superoxide dismutase (SOD) and glutathione (GSH) (Kurutas, 2015). In our study, we have observed that SOD (Fig. 3B) levels were significantly increased by BRD4-siRNA-LP treated animals as compared to LPS control group animals, however, there were no changes observed in PFI-1 treatment group. Apparently, we observed that both BRD4-siRNA-LP and PFI-1 moderately enhanced the GSH levels but not to a significant extent (Fig. 3C),

LPS induction increased IL-1 β (Fig. 3D), IL-6 (Fig. 3E), IL-17A (Fig. 3F), IL-22 (Fig. 3G), and TNF- α (Fig. 3H) levels, whereas these

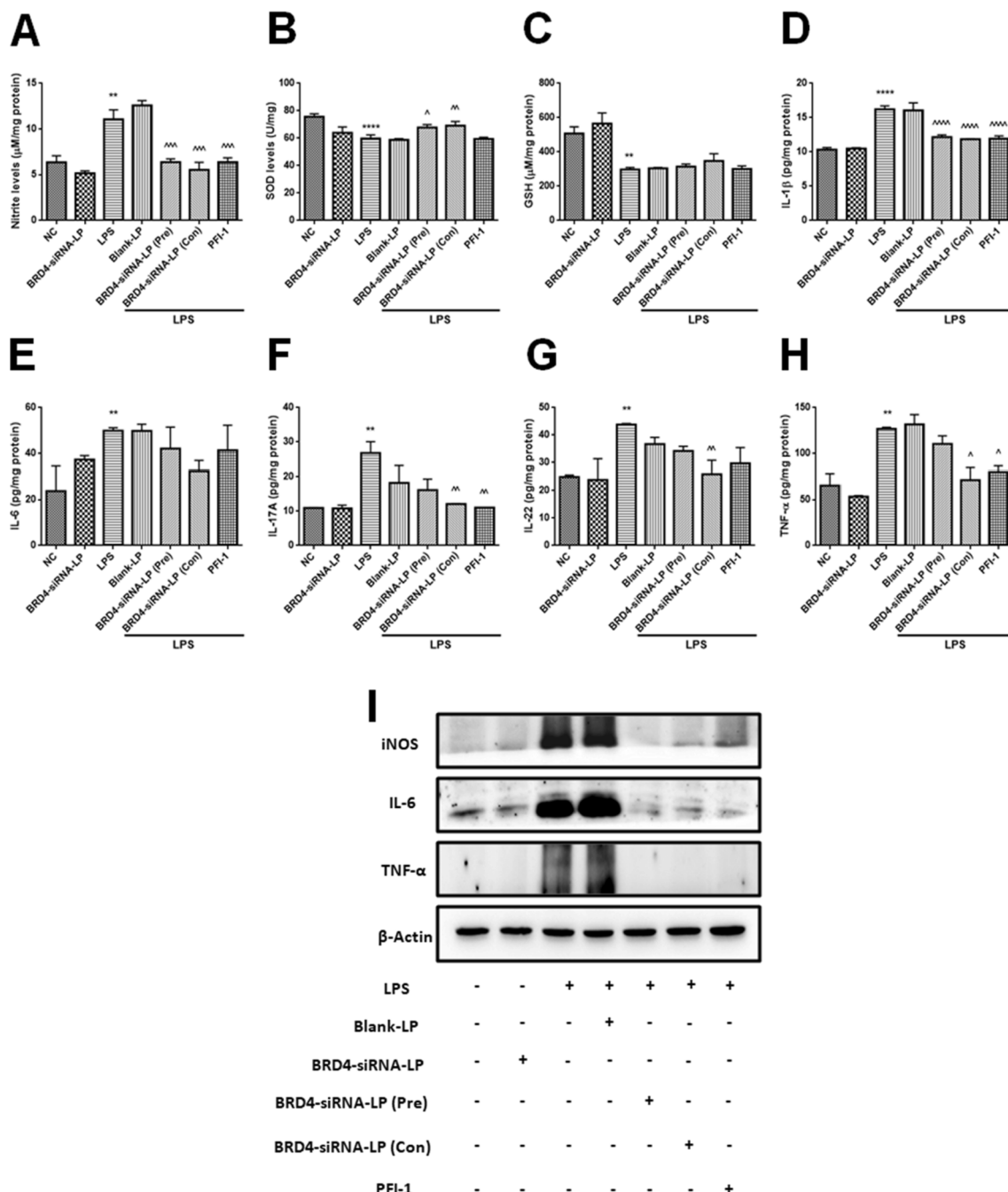


Fig. 3. BRD4-siRNA-LP suppress the nitrosative, oxidative stress, and cytokine storm in LPS induced ARDS mouse model. Mice were pretreated with BRD4-siRNA-LP and PFI-1, whereas the inflammation was induced by LPS oropharyngeal instillation. (A) Nitrite, (B) SOD, and (C) GSH levels were measured in lung tissues. The pro-inflammatory cytokine levels include (D) IL-1 β , (E) IL-6, (F) IL-17A, (G) IL-22, and (H) TNF- α were measured by ELISA in lung tissue lysates. (I) Additionally, the inflammatory iNOS, IL-6, and TNF- α protein expression was evaluated by western blotting. Data presented as mean \pm SD (n = 8 animals per group). **P < 0.01 and ****P < 0.0001 are significantly different from the NC group; ^P < 0.05, ^P < 0.01, ^P < 0.001, and ^P < 0.0001 are significantly different from the LPS group.

cytokines were significantly reduced by BRD4-siRNA-LP concurrent group, and showed superior effect compared to pre-treatment with siRNA lipoplexes and PFI-1. Here, PFI-1 slightly reduced IL-6 and IL-22 but non-significant. BRD4-siRNA-LP alone group did not induce the pro-inflammatory cytokines and the levels were in the normal range. Furthermore, we evaluated the expression of iNOS, TNF- α , and IL-6 by immunoblotting. Fig. 3I and Figure S2A-C infers that targeting BRD4 with lipoplexes as well as PFI-1 significantly suppressed the LPS induced iNOS, IL-6, and TNF- α expression, whereas BRD4-siRNA-LP alone group did not alter the expression of these inflammatory proteins. Collectively,

targeted inhibition of BRD4 and inhibiting the expression by BRD4-siRNA-LP hampers the cytokine storm, and we speculate that it has beneficial effects in protecting the lungs from COVID-19 associated respiratory failure.

3.4. BRD4-siRNA-LP modulate the LPS induced histopathological changes in LPS stimulated mice

Excessive inflammatory cytokines promote neutrophil infiltration and mast cell accumulation, which is responsible for respiratory illness

(Moldoveanu et al., 2008). The clinical sign of neutrophilia has been demonstrated the indicator of COVID-19 associated respiratory illness (Cavalcante-Silva et al., 2021). The recent reports infer that COVID-19 associated clinical subjects showed enhanced mast cells (Ribeiro dos Santos Miggioraro et al., 2020). Histopathological studies such as H&E (Fig. 4A and Figure S1B) and toluidine blue (Fig. 4B and Figure S1C) staining and microscopic observations show an increase in the neutrophils and mast cell number in both LPS and Blank-LP with concurrent changes in lung histology that reveal the extent of lung damage. By targeting BRD4, a remarkable improvement in pathological changes with a reduction in neutrophil infiltration and mast cell accumulation was observed. Moreover, we found that when compared to the BRD4-siRNA-LP pre-treatment group, concurrent group exhibited a more significant reduction in contrast to the LPS challenged group. Furthermore, epithelial barrier dysfunction was indistinguishable in BRD4-siRNA-LP alone group with normal pulmonary architecture. However, PFI-1 treatment exhibited similar results, but in comparison, BRD4-siRNA-

LP exhibited better effects. Thus, BRD4 inhibition mitigated the LPS induced alveolar disruption and further protected against pulmonary edema and alveolar damage.

3.5. BRD4-siRNA-LP inhibit LPS induced oxidative stress through the inhibition of Akt/MAPK signaling

The next goal of this study was to evaluate the molecular mechanism by BRD4-siRNA-LP in lung inflammation. The oxidative stress plays a crucial role in exacerbating ARDS and further involve in cytokine mediated inflammation (Kellner et al., 2017). To examine this effect; the *in vitro* experimentation was performed in RAW 264.7 cells. Initially, BRD4 knockdown studies were performed by treating the cells with different concentrations of BRD4-siRNA-LP at 1, 2.5, 5, and 10 nM and incubated for 48 h, then stimulated with LPS for 30 min. Then we quantified the BRD4 protein expression and observed a significant knockdown of BRD4 expression at 10 nM (Fig. 5A and Figure S3A) and

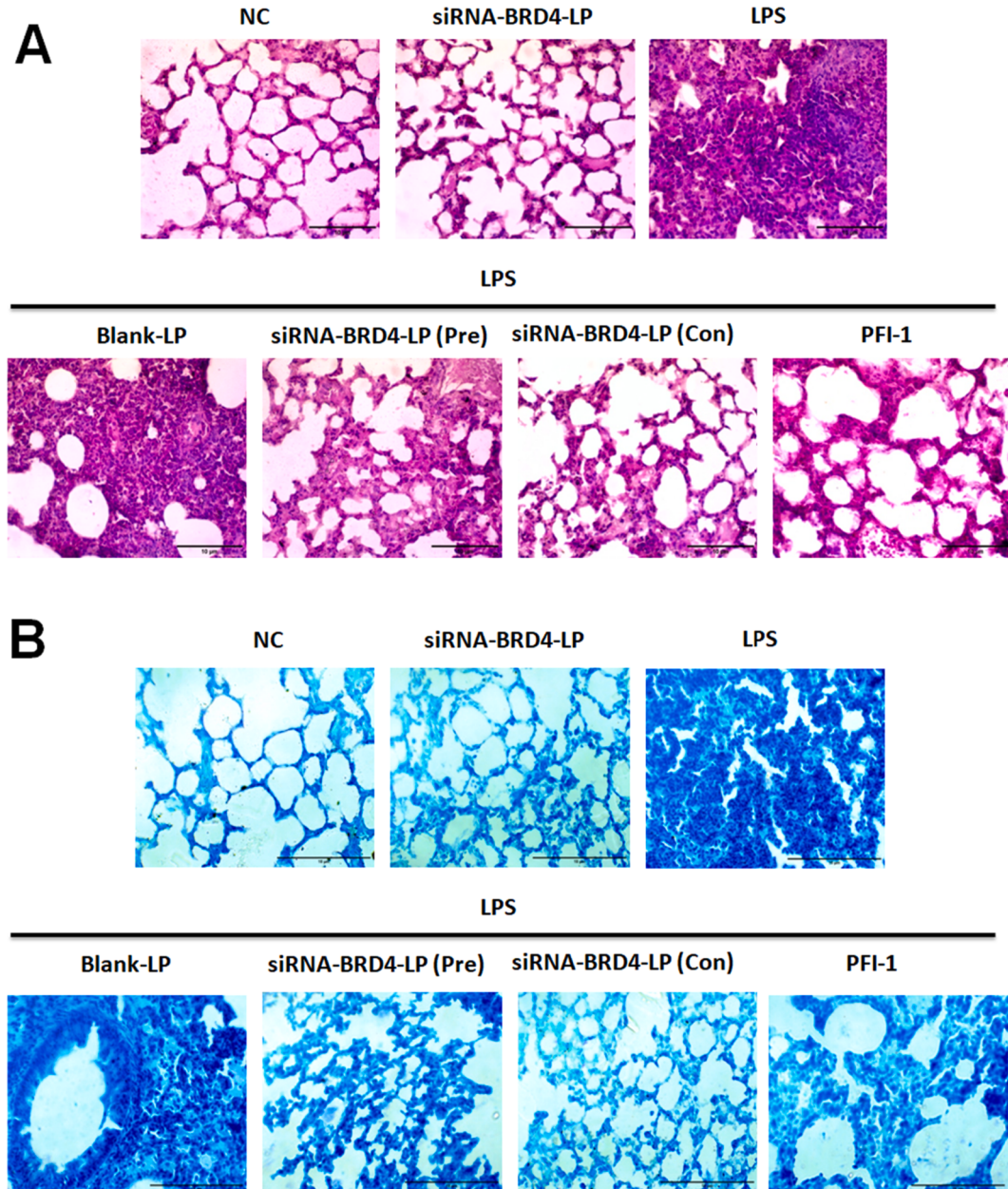


Fig. 4. BRD4-siRNA-LP inhibit LPS induced inflammatory and mast cell accumulation. The 5 μ m sized lung tissues were subjected to (A) H & E staining and (B) toluidine blue staining. The pathological changes were observed under the microscope and images were captured at $\times 400$ magnification.

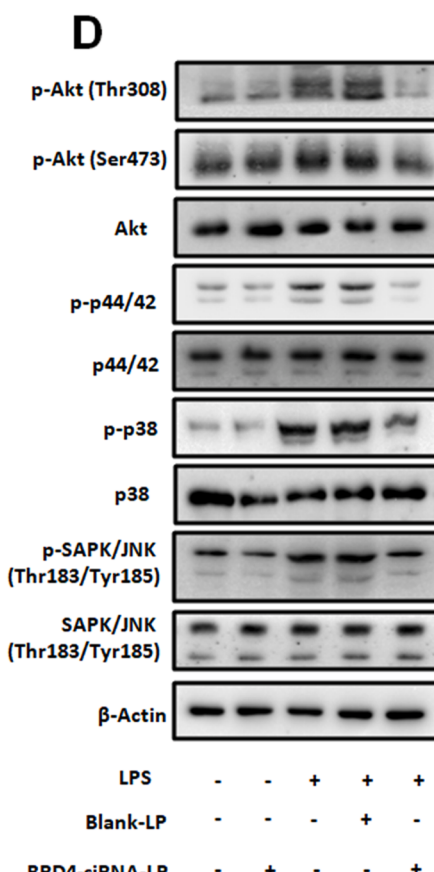
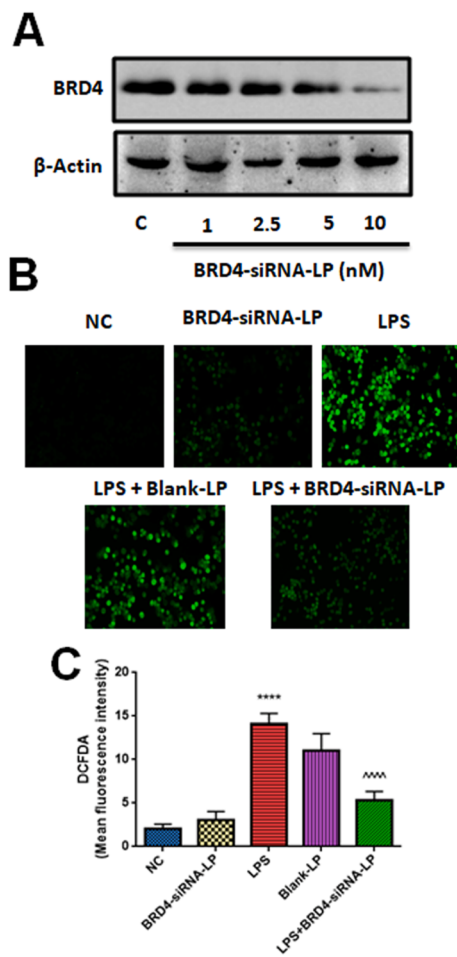


Fig. 5. BRD4-siRNA-LP show antioxidant effect by downregulating Akt/MAPK signaling in mouse macrophages. (A) Initially, RAW 264.7 cells were treated with BRD4-siRNA-LP (1, 2.5, 5, and 10 nM) for 48 h and expression of BRD4 investigated using western blotting. RAW 264.7 cells were pretreated with BRD4-siRNA-LP for 48 h and later cells were stimulated with LPS for 30 min. (B) The intracellular ROS levels were determined by DCFDA staining. The images were taken by fluorescent microscope at $\times 200$ magnification and (C) DCFDA intensity was measured by Image J, NIH, USA software. (C) Similarly, the phosphorylation of Akt (both Thr308 and Ser473 sites), p38, p44/42, and SAPK/JNK were determined by immunoblotting. Data presented as mean \pm SD ($n = 3$ independent experiments). *** $P < 0.0001$ is significantly different from the NC group; ** $P < 0.0001$ is significantly different from the LPS group.

further studies were executed with this concentration. LPS induced oxidative damage in macrophages at 1 μ g/ml, while in BRD4-siRNA-LP transfection at 10 nM concentration resulted in significant decreased the ROS levels, and no distinguishable changes occurred in the BRD4-siRNA-LP alone treatment (Fig. 5B & C). We next explored whether BRD4 has a direct impact on Akt and MAPK signaling using a loss of function of BRD4 by BRD4-siRNA-LP as it plays a crucial role in both inflammation and aggravate respiratory illness and LPS mimics this condition. It was found that LPS induced Akt (at Thr308 and Ser473), p38, p44/42, SAPK/JNK phosphorylation, where activation was also found with Blank-LP, and knock down of BRD4 significantly inhibited protein expression (Fig. 5D and Figure S3B-C). These results show that BRD4 is a selective target for oxidative stress and inflammation in ARDS.

3.6. BRD4 inhibition suppressed the Akt/mTOR/MAPK signaling in LPS challenged mice

Previous reports suggest that the anti-inflammatory potential of BET bromodomain binding to acetylated histones disrupt the LPS-induced expression of inflammatory cytokines and the formation of the chromatin complexes (Nicodeme et al., 2010). Consistently we observed that LPS enhanced the BRD4 mediated inflammation in ARDS mouse model, and was involved in the upregulation of Akt (Thr308 and Ser473), mTOR and GSK-3 β phosphorylation (Fig. 6A and Figure S4A-E). However, targeting BRD4 with BRD4-siRNA-LP and PFI-1 suppressed these inflammatory genes expression. Additionally, BRD4-siRNA-LP and PFI-1 inhibited the LPS induced phosphorylation of SAPK/JNK, p44/42, and p38 (Fig. 6B and Figure S4F-H). Here, we observed that BRD4-siRNA-LP showed superior activity over PFI-1 treatment, and BRD4-siRNA-LP

alone did not promote the activation of inflammatory cascade in the mouse upon oropharyngeal administration of LPS. Thus, targeting BRD4 inhibits the Akt/mTOR/MAPK signaling and ameliorates the LPS induced ARDS. P

3.7. BRD4-siRNA-LP inhibit LPS/TLR-4 mediated inflammation in macrophages by suppressing p65 and STAT3 nuclear translocation

TLR-4 agonist LPS induces the inflammation by stimulating the p65 NF- κ B signaling and causes severe respiratory illness. In our study, we found that LPS induced the phosphorylation of IKK- α/β , I κ B- α , p65 NF- κ B, and STAT3, which were significantly inhibited by BRD4-siRNA-LP (Fig. 7A and Figure S5A-D). Additionally, we observed that LPS induced nuclear p65 NF- κ B and STAT3 protein expression was significantly ameliorated by BRD4-siRNA-LP (Fig. 7B and Figure S5E & F). The transcriptional factors, p65 and STAT3, did not exhibit activity when they reside in the cytoplasm. However, these transcriptional factors were phosphorylated in the presence of inflammatory stimuli, and then enter into the nucleus, where they induced the expression of a wide variety of inflammatory genes, which are responsible for the respiratory collapse. Confocal microscopy results infer that LPS induced nuclear translocation of p65 and STAT3 is significantly downregulated by BRD4-siRNA-LP (Fig. 7C). Collectively, BRD4-siRNA-LP ameliorated the LPS induced ARDS by suppressing p65 and STAT3 crosstalk.

3.8. Targeting BRD4 inhibits p65 and STAT3 nuclear translocation in LPS induced ARDS mouse model

TLR-4 agonist LPS activated TRAF-6 mediated p65 signaling and

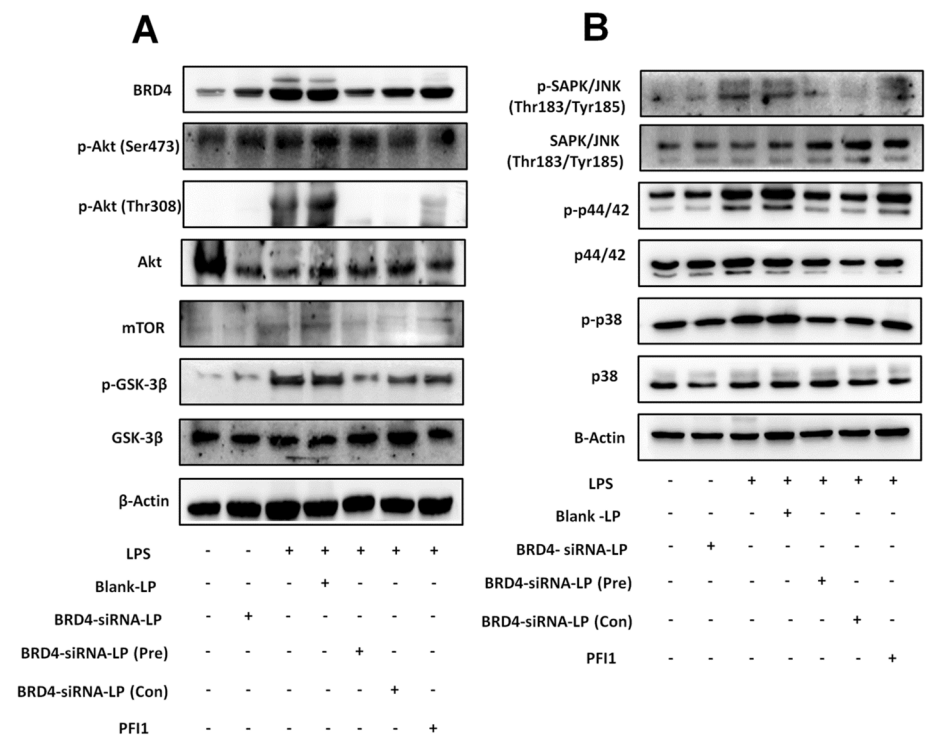


Fig. 6. BRD4-siRNA-LP suppress Akt/mTOR/MAPK signaling in LPS challenged mice. Mice were pretreated with 500 nM concentration of BRD4-siRNA-LP (pretreatment and concurrent) and PFI1 (5 mg/kg) for 2 h and later mice were stimulated with LPS for 12 h. Later protein was isolated from lung tissues and evaluated the (A) Akt and GSK-3 β phosphorylation, mTOR expression as well as (B) MAPK signaling by western blotting.

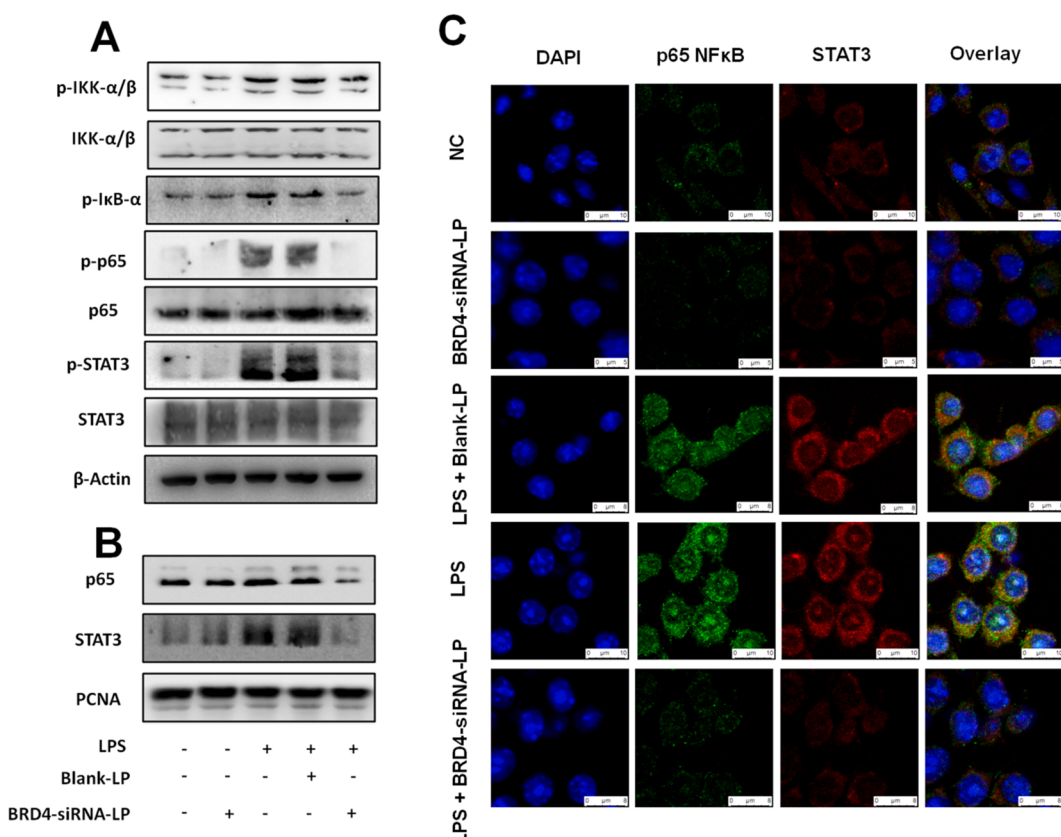


Fig. 7. BRD4-siRNA-LP inhibit p65 and STAT3 nuclear translocation. RAW 264.7 cells were pretreated with 10 nM of BRD4-siRNA-LP for 48 h and later cells were stimulated with 1 μ g/ml of LPS for 30 min. Protein lysates were isolated and subjected to SDS-PAGE. (A) Phosphorylation of IKK- α/β , I κ B- α , p65, and STAT3 and (B) nuclear p65 and STAT3 protein expression was evaluated by western blotting. (C) Nuclear translocation of p65 and STAT3 was studied by confocal microscopy. The images were captured at $\times 630$ magnification.

actively participated in inflammatory signaling cascade observed in C57/BL6 mice. Targeting BRD4 with novel drug delivery system BRD4-siRNA-LP and small-molecule inhibitor PFI-1 inhibited the phosphorylation of IKK- α/β , I κ B- α , p65 and STAT3 along with TRAF6 expression. However, the Blank-LP group did not reverse the LPS mediated changes and BRD4-siRNA-LP alone did not produce any inflammation and remained similar as NC (Fig. 8A and Figure S6A-E). Similar to *in vitro* results, here, we observed that BRD4-siRNA-LP suppressed LPS induced nuclear p65 NF- κ B and STAT3 expression (Fig. 8B and Figure S6F & G). Additionally, BRD4-siRNA-LP inhibited the nuclear translocation of p65 and STAT3 in LPS challenged mice (Fig. 8C). We also noticed that the small molecule inhibitor PFI-1 significantly inhibited the expression of p65 NF- κ B and STAT3. Collectively, BRD4 is a novel target, which is upregulated by inflammatory stimulus and induces the nuclear translocation of p65 and STAT3. Thus targeting it by novel lipoplex delivery system will be an useful aid for treating COVID-19 associated ARDS.

4. Discussion

Acute respiratory distress syndrome (ARDS) is a severe form of lung injury in critically ill patients. It is caused by higher levels of free reactive oxygen species and nitrogen species and is responsible for the activation of various inflammatory mediators leading to hypoxic pulmonary edema, and the need for mechanical ventilation (Kellner et al., 2017; Ricciardolo et al., 2006). ARDS most often occur with severe trauma, pneumonia, aspiration of gastric contents, bacterial sepsis or with viral infections from human coronaviruses such as severe acute respiratory syndrome coronavirus (SARS-CoV), middle east respiratory syndrome coronavirus (MERS-CoV) and a recent outbreak from COVID-19 associated novel coronavirus SARS-CoV-2 infections, which can progress to refractory pulmonary failure and ultimately increases

mortality rates (Petrosillo et al., 2020; Naeem, 2013). Despite its high incidence, there are no specific approved drugs to treat this condition. Supportive therapies such as restrictive fluid therapy, extracorporeal membrane oxygenation (ECMO) and prone positioning are some of the management strategies. These interventions improve the ARDS outcome but do not reduce the lung injury burden (Peck and Hibbert, 2019). In ARDS conditions, persistent inflammatory responses are observed as the air spaces are predominantly filled with infiltration of macrophages and neutrophils (Baudouin, 2006). In an attempt to improve the outcome, corticosteroid treatment was analyzed in ARDS patients, but their efficacy and beneficial effects in patients are divergent and controversial (Khilnani and Hadda, 2011). Unfortunately, sometimes ventilation also exacerbates ARDS by perpetuating local and systemic inflammation that further increases the mortality rates (Hough, 2014; Joseph et al., 2018). Recently, in COVID-19 induced ARDS cases, Aviptadil, a synthetic form of human vasoactive intestinal polypeptide (VIP) and Ruxolitinib, a selective Janus kinase (JAK) inhibitor are being investigated for ARDS treatment, which are under clinical trials (NCT04311697) (NCT04359290). However, there is still a huge scope to find new therapeutic targets and new drugs for this devastating ARDS condition (Mahase, 2020).

The structural motif, BRD4 is a member of the BET family that recognizes acetyl-lysine residues in both histone and non-histone proteins that orchestrate gene transcription by functioning as “readers”. BRD4 is implicated in several lung disease conditions such as chronic obstructive pulmonary disease (COPD), pulmonary fibrosis (Tian et al., 2016), lung cancer (Gao et al., 2018) and, asthma (Sanders and Thannickal, 2019). In the present study, we demonstrated for the first time that BRD4 has a predominant role in exacerbating inflammatory conditions, and thereby promotes ARDS. Further, the inhibition of BRD4 by chemical inhibitor PFI-1 and siRNA approaches were done and explained in preclinical

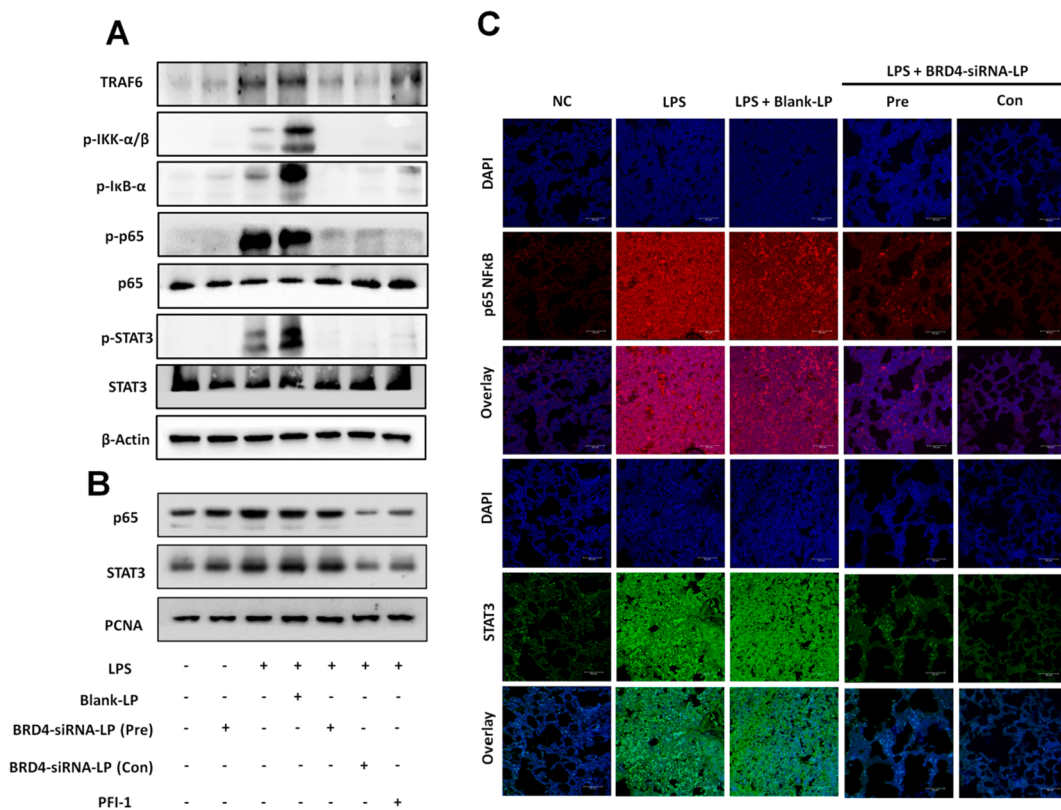


Fig. 8. BRD4-siRNA-LP inhibit LPS induced NF- κ B signaling and inhibited nuclear translocation of p65 and STAT3 signaling *in vivo*. C57/BL6 mice were treated with 500 nM of BRD4-siRNA-LP and 5 mg/kg of PFI-1. Further inflammation was induced by LPS instillation. (A) Western blotting was performed to evaluate the expression of TRAF6 and phosphorylation of IKK- α/β , I κ B- α , p65, and STAT3. (B) Nuclear p65 and STAT3 protein expression was studied by immunoblotting. (C) The nuclear translocation of p65 and STAT3 was evaluated by confocal microscopy. The images were captured at $\times 400$ magnification.

ARDS model. siRNA acts by RNA interference mechanisms, where it recognises the homologous mRNA sequence in the cell and further induces its degradation and this processes is selective in nature, whereas the chemical small molecular inhibitors suppress not only the target protein expression and also involve in downregulating other proteins and also having various side effects (Chernikov et al., 2019). In the current study, first time, we developed the BRD4-siRNA-LP, where observed the effect of this formulation in ameliorating LPS induced ARDS and its complications by delivering oropharyngeal route of administration. Here, BRD4 siRNA was encapsulated as stable cationic lipoplexes by thin-film hydration method with an equal ratio of cationic lipid DOTAP and neutral charge cholesterol. Here, DOTAP is used to incorporate the positive charge to the lipoplexes, whereas cholesterol is used to maintain stability by ensuring the neutral charge. Both Blank-LP and BRD4-siRNA-LP showed nano size and exhibited positive charge with acceptable PDI. The gel retardation assay results suggest that siRNA forms stable ionic interactions at 1:200 siRNA and lipid ratio, and showed $85.65 \pm 0.98\%$ entrapment efficiency. These lipoplexes were stable even in the presence of RNase. These siRNA lipoplexes were found to be stable in both *in vitro* and *in vivo*. *In vivo*, lipoplexes were administered via the oropharyngeal route for treating LPS induced respiratory complications. It is affirmed that preclinical demonstration of this novel delivery system will show the way for development of inhalational formulations for ARDS.

Although there are divergent causes for ARDS conditions, a series of acute inflammatory signaling cascades by evoking neutrophil infiltration, mast cell accumulation, oxidative and nitrosative stress, cytokine storm, damage to the epithelial and endothelial cells and respiratory illness are the common manifestations. The LPS induced ARDS model was selected in this study as it is a widely accepted model ,and mimics most of the symptoms of ARDS that are commonly seen in sepsis and COVID-19 conditions (Coperchini et al., 2020; Domscheit et al., 2020). From a pathophysiological perspective, both LPS and COVID19-associated lung inflammation shows ARDS symptoms such as pulmonary edema, endothelial inflammation, impaired pulmonary physiology, altered alveolar homeostasis and infiltration of inflammatory cytokines (Pfortmueller et al., 2020).

Previous reports suggest that the LPS stimulation induces an increase in BRD4 binding with genes, and it has been reported that signal intensity of BRD4 increased with LPS stimulation and BRD4 in macrophages is essential for eliciting TLR Signaling (Dey et al., 2019; Bao et al., 2017) Moreover, Gordon et al. suggest that SARS-CoV-2 transmembrane protein E binds with BRD2 and BRD4, thus, targeting BRD4 may inhibit the viral fusion into host cells as well as respiratory illness (Gordon et al., 2020). These findings raise an intriguing possibility that BRD4 might be involved in ARDS conditions. Consistent with this expectation, after LPS oropharyngeal instillation, the net body weights were found to be decreased, whereas increased lung weight index was observed. Interestingly, BRD4-siRNA-LP treated groups, there were no major physiological alterations. Moreover, BRD4-siRNA-LP suppressed the LPS induced total cells, WBC, neutrophils, monocytes, and basophils counts, and protected the epithelial barrier dysfunction. In ARDS patients cytokines such as TNF- α , IL-1 β , IL-6, and IL-8 are elevated in BAL fluid and circulating plasma (Han and Mallampalli, 2015). In COVID-19 associated critically ill patients in Intensive care unit (ICU) wards, higher plasma levels of various inflammatory cytokines including MCP -1, MIP -1A, GSCF, TNF- α , IL -2, IL -7, IL -10, and IP -10 were observed (Pooladanda et al., 2020). This cytokine storm perpetuates inflammatory immune cell infiltration, causes accumulation of protein-rich edema fluid into the alveoli with hypoxemia which is caused due to impairment of gas exchange (Pedersen and Ho, 2020). Hence, antioxidant therapy might be useful in ameliorating the ARDS condition (Wang et al., 2020). Here, LPS induced the nitrite levels and reduced the SOD and GSH levels, whereas BRD4-siRNA-LP inhibited nitrosative and oxidative stress by upregulating the antioxidant defensive mechanism. BRD4-siRNA-LP reversed the LPS induced cytokine storm by

significantly suppressing pro-inflammatory cytokine levels including IL-1 β , IL-6, IL-17A, IL22, and TNF- α . From H & E and Toluidine blue staining, it was observed that BRD4-siRNA-LP suppressed the LPS induced neutrophil and mast cell infiltration and protected the lungs from immune cell-mediated cytokine storm.

Targeting BRD4 suppresses the PI3K-Akt/MAPK/JNK signaling in cancer and inflammatory diseases, and these pathways important in the regulation of inflammatory responses (Liu et al., 2018; Stratikopoulos et al., 2015; Wang et al., 2018). In line with this, previous reports suggest that JNK, p38, and PI3K/Akt were involved in severe acute respiratory distress syndrome-coronavirus (SARS-CoV) infected Vero E6 cells, which suggest the possible involvement of inflammation in COVID-19 associated ARDS through this signaling (Mizutani et al., 2005). BRD4-siRNA-LP potently inhibited the LPS induced mTOR expression and phosphorylation of Akt at Thr308 and Ser473. Additionally, targeting BRD4 suppressed the LPS induced phosphorylation of p44/42, p38, GSK-3 β , and SAPK/JNK.

On the other hand, SARS-CoV-2 activates p65 NF- κ B signaling similar to SARS-CoV and the Middle East respiratory syndrome-coronavirus (MERS-CoV), which is critical for pulmonary inflammation and associated series of events (Chen et al., 2020). BRD4 coactivates the NF- κ B transcriptional activity by acetylating p65 also known as RelA (Huang et al., 2009). Upon I κ B- α degradation, p65 moves into the nucleus, and further induces the transcription of various inflammatory genes and evokes the ARDS (Moine et al., 2000). The accumulating evidence suggest that deletion of BRD4 in macrophages showed constant MAP kinase-interacting serine/threonine-protein kinase 2 (Mknk2) and involved in the activation of eIF4E, which further aided in I κ B- α mRNA translation, which ultimately suppressed the NF- κ B mediated inflammatory signaling and demonstrated that conditional knock out of BRD4 in mice were resistant to the sepsis conditions induced by LPS, which depicts the role of BRD4 in regulating the innate immune response (Bao et al., 2017). With respect to this paradigm, in our experimentation, we have observed that LPS induced the phosphorylation of IKK- α / β , I κ B- α , and p65, whereas this effect was significantly inhibited by BRD4-siRNA-LP. Accumulating evidence suggest that pro-inflammatory cytokine stimulus activates the STAT3 and NF- κ B crosstalk through TRAF6 and p65 dependent mechanism (Yoshida et al., 2004). On the other hand, STAT3 retains the nuclear-bounded p65, thus promotes persistent inflammation (Yu et al., 2009) In addition, targeting BRD4 inhibits the STAT3-dependent MYC expression in cancer, however, it is not yet elucidated in inflammatory condition (Ray et al., 2014). In our study, we noticed that BRD4 inhibition suppressed the STAT3 phosphorylation. We also observed that BRD4-siRNA-LP significantly inhibited p65 and STAT3 and further reduced the activation of inflammatory proteins expression. This might be therefore a promising novel target with the potentially advantageous delivery systems, which may be considered in treating COVID-19 induced ARDS (Fig. 9).

Collectively, our results infer that BRD4 is a novel target for ARDS irrespective of its origin. The LPS induced ARDS model may mimic the COVID-19 associated ARDS. Inhibition of BRD4 by BRD4-siRNA-LP might play an important role in treating clinical COVID-19-ARDS patients potentially through anti-inflammatory and anticytokine storm properties by controlling p65 and STAT3 nuclear translocation. Thus, it could be a better therapeutic strategy for treating COVID-19 induced ARDS in this global pandemic.

CRediT authorship contribution statement

Venkatesh Pooladanda: Conceptualization, Methodology, Writing - original draft, Software, Validation. **Sowjanya Thatikonda:** Visualization, Methodology, Writing - original draft. **Sai Priya Muvala:** Methodology. **Geetanjali Devabattula:** Methodology. **Chandraiah Godugu:** Supervision.

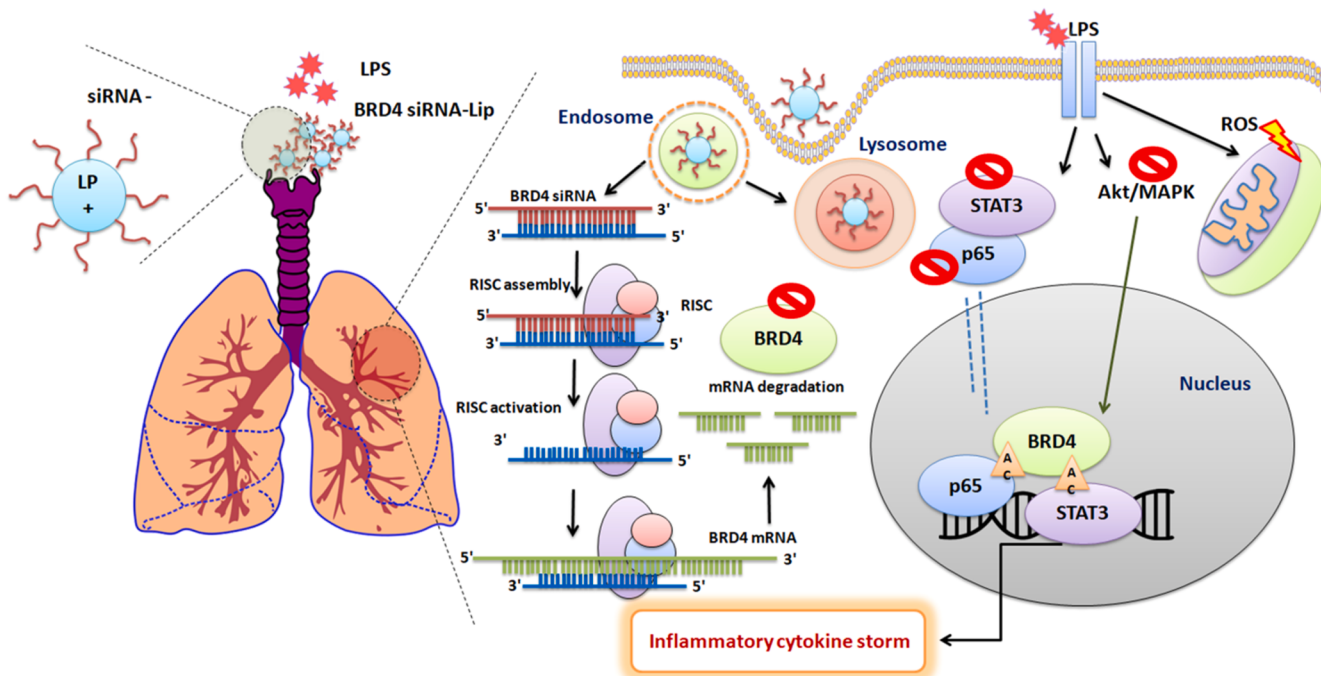


Fig. 9. A schematic diagram represents the therapeutic potential of BRD4-siRNA-LP in LPS-induced ARDS. The novel liposomal delivery system, BRD4-siRNA-LP suppress the oxidative stress, cytokine storm, and pulmonary inflammation by inhibiting the nuclear translocation and p65 and STAT3.

Declaration of Competing Interest

The authors declare that they have no known competing financial interests or personal relationships that could have appeared to influence the work reported in this paper.

Acknowledgements

Authors acknowledge the Director, NIPER, Hyderabad, India for supporting research activities. Authors thankful to Dr. Sheenam Beg, Government Medical College, Rajnandgaon, India, for helping in pathological scoring. Authors also acknowledge to Department of Pharmaceuticals (DoP), Ministry of Chemicals and Fertilizers, Government of India for providing research facilities.

Appendix A. Supplementary data

Supplementary data to this article can be found online at <https://doi.org/10.1016/j.ijpharm.2021.120536>.

References

- Alshehri, A., Grabowska, A., Stolnik, S., 2018. Pathways of cellular internalisation of liposomes delivered siRNA and effects on siRNA engagement with target mRNA and silencing in cancer cells. *Sci. Rep.* 8, 1–9. <https://doi.org/10.1038/s41598-018-22166-3>.
- Alvira, C.M., 2014. Nuclear factor-kappa-B signaling in lung development and disease: one pathway, numerous functions. *Birth Defects Res. A Clin. Mol. Teratol.* 100 (3), 202–216. <https://doi.org/10.1002/bdra.23233>.
- Bagaev, A.V., Garaeva, A.Y., Lebedeva, E.S., Pichugin, A.V., Ataullakhanov, R.I., Ataullakhanov, F.I., 2019. Elevated pre-activation basal level of nuclear NF- κ B in native macrophages accelerates LPS-induced translocation of cytosolic NF- κ B into the cell nucleus. *Sci. Rep.* 9, 1–16. <https://doi.org/10.1038/s41598-018-36052-5>.
- Bao, Y., Wu, X., Chen, J., Hu, X., Zeng, F., Cheng, J., Jin, H., Lin, X., Chen, L.-F., 2017. Brd4 modulates the innate immune response through Mnk2-eIF4E pathway-dependent translational control of I κ B α . *PNAS* 114 (20), E3993–E4001. <https://doi.org/10.1073/pnas.1700109114>.
- Baudouin, S.V., 2006. Manipulation of inflammation in ARDS: achievable goal or distant target? *Thorax* 61 (6), 464–465. <https://doi.org/10.1136/thx.2005.057265>.
- Bellani, G., Laffey, J.G., Pham, T., Fan, E., Brochard, L., Esteban, A., Gattinoni, L., van Haren, F., Larsson, A., McAuley, D.F., Ranieri, M., Rubenfeld, G., Thompson, B.T., Wrigge, H., Slutsky, A.S., Pesenti, A., LUNG SAFE Investigators, ESICM Trials group,
2016. Epidemiology, patterns of care, and mortality for patients with acute respiratory distress syndrome in intensive care units in 50 countries. *JAMA* 315, 788–800. <https://doi.org/10.1001/jama.2016.0291>.
- Cavalcante-Silva, Luiz Henrique Agra, Carvalho, Deyse Cristina Madruga, Lima, Éssia de Almeida, Galvão, José G.F.M., da Silva, Juliane S. de França, Sales-Neto, José Marreiro de, Rodrigues-Mascarenhas, Sandra, 2021. Neutrophils and COVID-19: The road so far. *Int. Immunopharmacol.* 90, 107233. <https://doi.org/10.1016/j.intimp.2020.107233>.
- Chen, B., Tian, E.K., He, B., Tian, L., Han, R., Wang, S., Xiang, Q., Zhang, S., El Arnaout, T., Cheng, W., 2020. Overview of lethal human coronaviruses. *Signal Transduct. Target Ther.* 5 (1), 1–6. In this issue.
- Chernikov, I.V., Vlassov, V.V., Chernolovskaya, E.L., 2019. Current development of siRNA bioconjugates: From Research to the Clinic. *Front. Pharmacol.* 10, 444. <https://doi.org/10.3389/fphar.2019.00444>.
- Cochran, A.G., Conery, A.R., Sims, R.J., 2019. Bromodomains: a new target class for drug development. *Nat. Rev. Drug Discovery* 18, 609–628. <https://doi.org/10.1038/s41573-019-0030-7>.
- Coperchini, F., Chiovato, L., Croce, L., Magri, F., Rotondi, M., 2020. The Cytokine storm in COVID-19: An overview of the involvement of the chemokine/chemokine-receptor system. *Cytokine Growth Factor Rev.* 53, 25–32. <https://doi.org/10.1016/j.cytofr.2020.05.003>.
- COVID-19 Map, n.d. Johns Hopkins Coronavirus Resource Center. <https://coronavirus.jhu.edu/map.html> (accessed 02.18.20).
- Dana, H., Chalbatani, G.M., Mahmoodzadeh, H., Karimloo, R., Rezaiean, O., Moradzadeh, A., Mehmandoost, N., Moazzen, F., Mazraeh, A., Marmari, V., Ebrahimi, M., Rashno, M.M., Abadi, S.J., Gharagouzlo, E., 2017. Molecular mechanisms and biological functions of siRNA. *Int. J. Biomed. Sci.* 13, 48–57.
- Deshpande, Pranali P., Biswas, Swati, Torchilin, Vladimir P., 2013. Current trends in the use of liposomes for tumor targeting. *Nanomedicine (Lond)* 8 (9), 1509–1528. <https://doi.org/10.2217/nmm.13.118>.
- Dey, A., Yang, W., Gegonne, A., Nishiyama, A., Pan, R., Yagi, R., Grinberg, A., Finkelman, F.D., Pfeifer, K., Zhu, J., Singer, D., Zhu, J., Ozato, K., 2019. BRD4 directs hematopoietic stem cell development and modulates macrophage inflammatory responses. *EMBO J.* 38. <https://doi.org/10.15252/embj.2018100293> e100293.
- Diamond, M., Peniston Feliciano, H.L., Sanghavi, D., Mahapatra, S., 2020. Acute Respiratory Distress Syndrome (ARDS), in: StatPearls. StatPearls Publishing, Treasure Island (FL).
- Domscheit, H., Hegeman, M.A., Carvalho, N., Spieth, P.M., 2020. Molecular Dynamics of Lipopolysaccharide-Induced Lung Injury in Rodents. *Front. Physiol.* 11, 36. <https://doi.org/10.3389/fphys.2020.00036>.
- Duan, Yingchao, Guan, Yuanyuan, Qin, Wenping, Zhai, Xiaoyu, Yu, Bin, Liu, Hongmin, 2018. Targeting Brd4 for cancer therapy: inhibitors and degraders. *Medchemcomm* 9 (11), 1779–1802. <https://doi.org/10.1039/C8MD00198G>.
- Fujiwara, N., Kobayashi, K., 2005. Macrophages in inflammation. *Curr. Drug Targets Inflamm. Allergy* 4, 281–286. <https://doi.org/10.2174/1568010054022024>.
- Gao, Zhongyuan, Yuan, Ting, Zhou, Xiao, Ni, Ping, Sun, Geng, Li, Ping, Cheng, Zhixiang, Wang, Xuerong, 2018. Targeting BRD4 proteins suppresses the growth of NSCLC through downregulation of eIF4E expression. *Cancer Biol. Ther.* 19 (5), 407–415. <https://doi.org/10.1080/15384047.2018.1423923>.

- Gordon, D.E., Jang, G.M., Bouhaddou, M., Xu, J., Obernier, K., O'Meara, M.J., Guo, J.Z., Swaney, D.L., Tummino, T.A., Huettenhain, R., Kaake, R.M., Richards, A.L., Tutuncuoglu, B., Foussard, H., Batra, J., Haas, K., Modak, M., Kim, M., Haas, P., Polacco, B.J., Braberg, H., Fabius, J.M., Eckhardt, M., Soucheray, M., Bennett, M.J., Cakir, M., McGregor, M.J., Li, Q., Naing, Z.Z.C., Zhou, Y., Peng, S., Kirby, I.T., Melnyk, J.E., Chorba, J.S., Lou, K., Dai, S.A., Shen, W., Shi, Y., Zhang, Z., Barrio-Hernandez, I., Memon, D., Hernandez-Armenta, C., Mathy, C.J.P., Perica, T., Pilla, K., B., Ganesan, S.J., Saltzberg, D.J., Ramachandran, R., Liu, X., Rosenthal, S.B., Calviello, L., Venkataramanan, S., Liboy-Lugo, J., Lin, Y., Wankowicz, S.A., Bohn, M., Sharp, P.P., Trenker, R., Young, J.M., Cavero, D.A., Hiatt, J., Roth, T.L., Rathore, U., Subramanian, A., Noack, J., Hubert, M., Roesch, F., Vallet, T., Meyer, B., White, K.M., Miorin, L., Rosenberg, O.S., Verba, K.A., Agard, D., Ott, M., Emerman, M., Ruggero, D., Garcia-Sastre, A., Jura, N., Zastrow, M., von, Taunton, J., Ashworth, A., Schwartz, O., Vignuzzi, M., d'Enfert, C., Mukherjee, S., Jacobson, M., Malik, H.S., Fujimori, D.G., Ideker, T., Craik, C.S., Floor, S., Fraser, J.S., Gross, J., Sali, A., Kortemme, T., Beltrao, P., Shokat, K., Shoichet, B.K., Krojan, N.J., 2020. A SARS-CoV-2-Human Protein-Protein Interaction Map Reveals Drug Targets and Potential Drug-Repurposing. *bioRxiv* 002386. <https://doi.org/10.1101/2020.03.22.002386>.
- Grinelli, Katie L., Chichger, Havovi, Braza, Julie, Duong, Hueteran, Harrington, Elizabeth O., 2012. Protection against LPS-induced pulmonary edema through the attenuation of protein tyrosine phosphatase-1B oxidation. *Am. J. Respir. Cell Mol. Biol.* 46 (5), 623–632. <https://doi.org/10.1165/rcmb.2011-0271OC>.
- Guha, Mausume, Mackman, Nigel, 2002. The phosphatidylinositol 3-Kinase-akt pathway limits lipopolysaccharide activation of signaling pathways and expression of inflammatory mediators in human monocytic cells. *J. Biol. Chem.* 277 (35), 32124–32132. <https://doi.org/10.1074/jbc.M203298200>.
- Hajmirza, A., Emadali, A., Gauthier, A., Casasnovas, O., Gressin, R., Callanan, M.B., 2018. BET family protein BRD4: An emerging actor in nfkb signaling in inflammation and cancer. *Biomedicines* 6, 16. <https://doi.org/10.3390/biomedicines6010016>.
- Han, SeungHye, Mallampalli, Rama K., 2015. The acute respiratory distress syndrome: from mechanism to translation. *J. Immunol.* 194 (3), 855–860. <https://doi.org/10.4049/jimmunol.1402513>.
- Hough, C.L., 2014. Should we ever give steroids to ARDS patients? *Clin. Chest Med.* 35, 781–795. <https://doi.org/10.1016/j.ccm.2014.08.014>.
- Huang, Bo, Yang, Xiao-Dong, Zhou, Ming-Ming, Ozato, Keiko, Chen, Lin-Feng, 2009. BRD4 coactivates transcriptional activation of NF- κ B via specific binding to acetylated RelA. *Mol. Cell. Biol.* 29 (5), 1375–1387. <https://doi.org/10.1128/MCB.01365-08>.
- Jain, Anjali, Pooladanda, Venkatesh, Bulbake, Upendra, Doppalapudi, Sindhu, Rafaeqi, Towseef Amin, Godugu, Chandraiah, Khan, Wahid, 2017. Liposphere mediated topical delivery of thymoquinone in the treatment of psoriasis. *Nanomedicine* 13 (7), 2251–2262. <https://doi.org/10.1016/j.nano.2017.06.009>.
- Joseph, A., Khan, M.F., Rajendram, R., 2018. Strategies to prevent ventilator-associated lung injury in critically ill patients. *Indian J. of Resp. Care* 7, 4.
- Kellner, M., Noonepalle, S., Lu, Q., Srivastava, A., Zemskov, E., Black, S.M., 2017. ROS signaling in the pathogenesis of acute lung injury (ALI) and acute respiratory distress syndrome (ARDS). *Adv. Exp. Med. Biol.* 967, 105–137. https://doi.org/10.1007/978-3-319-63245-2_8.
- Khilnani, G.C., Hadda, V., 2011. Corticosteroids and ARDS: A review of treatment and prevention evidence. *Lung India* 28, 114–119. <https://doi.org/10.4103/0970-2113.80324>.
- Klein, Kerstin, 2018. Bromodomain protein inhibition: a novel therapeutic strategy in rheumatic diseases. *RMD Open* 4 (2), e000744. <https://doi.org/10.1136/rmopen-2018-000744>.
- Kurutas, E.B., 2015. The importance of antioxidants which play the role in cellular response against oxidative/nitrosative stress: current state. *Nutri. J.* 15, 1–22.
- Li, J., Duan, Z., Guo, W., Zeng, L., Wu, Y., Chen, Y., Tai, F., Wang, Y., Lin, Y., Zhang, Q., He, Y., Deng, J., Stewart, R.L., Wang, C., Lin, P.C., Ghaffari, S., Evers, B.M., Liu, S., Zhou, M.-M., Zhou, B.P., Shi, J., 2018. Targeting the BRD4/FOXO3a/CDK6 axis sensitizes AKT inhibition in luminal breast cancer. *Nat. Commun.* 9, 1–17. <https://doi.org/10.1038/s41467-018-07258-y>.
- Mahase, E., 2020. Covid-19: what treatments are being investigated?. 368, m1252.
- Miller, T.C.R., Simon, B., Rybin, V., Grötsch, H., Curtet, S., Khochbin, S., Carlomagno, T., Müller, C.W., 2016. A bromodomain-DNA interaction facilitates acetylation-dependent bivalent nucleosome recognition by the BET protein BRDT. *Nat. Commun.* 7, 1–13. <https://doi.org/10.1038/ncomms1385>.
- Mizutani, Tetsuya, Fukushima, Shuetsu, Saito, Masayuki, Kurane, Ichiro, Morikawa, Shigeru, 2005. JNK and PI3k/Akt signaling pathways are required for establishing persistent SARS-CoV infection in Vero E6 cells. *BBA* 1741 (1-2), 4–10. <https://doi.org/10.1016/j.bbadiis.2005.04.004>.
- Möhlenkamp, Stefan, Thiele, Holger, 2020. Ventilation of COVID-19 patients in intensive care unitsBeatmung von COVID-19-Patienten auf Intensivstationen. *Herz* 45 (4), 329–331. <https://doi.org/10.1007/s00590-020-04923-1>.
- Moine, P., McIntyre, R., Schwartz, M.D., Kaneko, D., Shenkar, R., Le Tulzo, Y., Moore, E. E., Abraham, E., 2000. NF- κ B regulatory mechanisms in alveolar macrophages from patients with acute respiratory distress syndrome. *Shock* 13, 85–91. <https://doi.org/10.1097/00024382-200013020-00001>.
- Moldoveanu, B., Otmishi, P., Jani, P., Walker, J., Sarmiento, X., Guardiola, J., Saad, M., Yu, J., 2008. Inflammatory mechanisms in the lung. *J. Inflamm. Res.* 2, 1–11.
- Naeem, Z. 2014. Middle East Respiratory Syndrome (MERS) – An update, 2013. . *Int. J. Health Sci. (Qassim)* 7, V–VI.
- Nicodeme, Edwige, Jeffrey, Kate L., Schaefer, Uwe, Beinke, Soren, Dewell, Scott, Chung, Chun-wa, Chandwani, Rohit, Marazzi, Ivan, Wilson, Paul, Coste, Hervé, White, Julia, Kirillovsky, Jorge, Rice, Charles M., Lora, Jose M., Prinjha, Rab K., Lee, Kevin, Tarakhovsky, Alexander, 2010. Suppression of inflammation by a synthetic histone mimic. *Nature* 468 (7327), 1119–1123. <https://doi.org/10.1038/nature09589>.
- Pal Singh, Pirthi, Vithalapuram, Veena, Metre, Sunita, Kodipiyaka, Ravinder, 2020. Lipoplex-based therapeutics for effective oligonucleotide delivery: a compendious review. *J. Liposome Res.* 30 (4), 313–335. <https://doi.org/10.1080/08982104.2019.1652645>.
- Pandi, Palpandi, Jain, Anjali, Kommineni, Nagavendra, Ionov, Maksim, Bryszewska, Maria, Khan, Wahid, 2018. Dendrimer as a new potential carrier for topical delivery of siRNA: A comparative study of dendriplex vs. lipoplex for delivery of TNF- α siRNA. *Int. J. Pharm.* 550 (1-2), 240–250. <https://doi.org/10.1016/j.ijpharm.2018.08.024>.
- Patil, S., Yi, J., Bang, E.-K., Jeon, E., Kim, B., 2011. Synthesis and efficient siRNA delivery of polyamine-conjugated cationic nucleoside lipids. *Med. Chem. Commun.* 2, 505–508. <https://doi.org/10.1039/C1MD00014D>.
- Peck, T.J., Hibbert, K.A., 2019. Recent advances in the understanding and management of ARDS. *F1000Res* 8. <https://doi.org/10.12688/f1000research.20411.1>.
- Pedersen, S.H., Ho, Y.C., 2020. SARS-CoV-2: a storm is raging. *J. Clin. Invest.* 130, 2202–2205. <https://doi.org/10.1172/JCI137647>.
- Petrosillo, N., Viceconte, G., Ergonul, O., Ippolito, G., Petersen, E., 2020. COVID-19, SARS and MERS: are they closely related? *Clin. Microbiol. Infect.* 26 (6), 729–734. <https://doi.org/10.1016/j.cmi.2020.03.026>.
- Pfortmueller, C.A., Spinetti, T., Urman, RD., Luedi, MM., Schefold, JC., 2020. COVID-19 associated acute respiratory distress syndrome (ARDS): current knowledge on pathophysiology and ICU treatment-a narrative review. *Best Pract. Res. Clin. Anaesthesiol.* <https://doi.org/10.1016/j.bpr.2020.12.011>. In press.
- Pooladanda, V., Thatikonda, S., Bale, S., Pattnaik, B., Sigalapalli, D.K., Bathini, N.B., Singh, S.B., Godugu, C., 2019. Nimolide protects against endotoxin-induced acute respiratory distress syndrome by inhibiting TNF- α mediated NF- κ B and HDAC-3 nuclear translocation. *Cell Death Dis.* 10, 81. <https://doi.org/10.1038/s41419-018-1247-9>.
- Pooladanda, Venkatesh, Thatikonda, Sowjanya, Godugu, Chandraiah, 2020. The current understanding and potential therapeutic options to combat COVID-19. *Life Sci.* 254, 117765. <https://doi.org/10.1016/j.lfs.2020.117765>.
- Pooladanda, Venkatesh, Thatikonda, Sowjanya, Sunnapa, Omprakash, Tiwary, Shristy, Vemula, Praveen Kumar, Talluri, M V N Kumar, Godugu, Chandraiah, 2021. iRGD conjugated nimolide liposomes protect against endotoxin induced acute respiratory distress syndrome. *Nanomedicine* 33, 102351. <https://doi.org/10.1016/j.nano.2020.102351>.
- Pu, D., Wang, W., 2014. Toll-like receptor 4 agonist, lipopolysaccharide, increases the expression levels of cytokines and chemokines in human peripheral blood mononuclear cells. *Exp. Ther. Med.* 8, 1914–1918. <https://doi.org/10.3892/etm.2014.2025>.
- Qiu, Yingshan, Lam, Jenny, Leung, Susan, Liang, Wanling, 2016. Delivery of RNAi therapeutics to the airways—from bench to bedside. *Molecules* 21 (9), 1249. <https://doi.org/10.3390/molecules21091249>.
- Ray, Sutapa, Zhao, Yingxin, Jamaluddin, Mohammad, Edeh, Chukwudi B., Lee, Chang, Brasier, Allan R., 2014. Inducible STAT3 NH2 Terminal mono-ubiquitination promotes BRD4 complex formation to regulate apoptosis. *Cell. Signal.* 26 (7), 1445–1455. <https://doi.org/10.1016/j.cellsig.2014.03.007>.
- Ribeiro dos Santos Miggioraro, Anna Flavia, da Silva Motta Junior, Jarbas, Busatta Vaz de Paula, Caroline, Nagashima, Seigo, Alessandra Scaranello Malaquias, Mineia, Baena Carstens, Lucas, N Moreno-Amaral, Andrea, Pellegrino Baena, Cristina, de Noronha, Lucia, 2020. Covid-19 cytokine storm in pulmonary tissue: Anatomopathological and immunohistochemical findings. *Respir. Med. Case Rep.* 31, 101292. <https://doi.org/10.1016/j.rimcr.2020.101292>.
- Ricciardolo, Fabio L.M., Di Stefano, Antonino, Sabatini, Federica, Folkerts, Gert, 2006. Reactive nitrogen species in the respiratory tract. *Eur. J. Pharmacol.* 533 (1-3), 240–252. <https://doi.org/10.1016/j.ejphar.2005.12.057>.
- Sanders, Yan Y., Thannickal, Victor J., 2019. BETting on Novel Treatments for Asthma: Bromodomain 4 Inhibitors. *Am. J. Respir. Cell Mol. Biol.* 60 (1), 7–8. <https://doi.org/10.1165/rmbc.2018-0271ED>.
- Schroeder, A., Levins, C.G., Cortez, C., Langer, R., Anderson, D.G., 2010. Lipid-based nanotherapeutics for siRNA delivery. *J. Intern. Med.* 267, 9–21. <https://doi.org/10.1111/j.1365-2796.2009.02189.x>.
- Selvaraj, V., Nepal, N., Rogers, S., Manne, N.D.P.K., Arvapalli, R., Rice, K.M., Asano, S., Fankenhanel, E., Ma, J.Y., Shokuhfar, T., Maheshwari, M., Blough, E.R., 2015. Lipopolysaccharide induced MAP kinase activation in RAW 264.7 cells attenuated by cerium oxide nanoparticles. *Part. Part. Syst. Charact.* 38, 96–99. <https://doi.org/10.1016/j.dib.2015.04.022>.
- Shim, Gayong, Kim, Mi-Gyeong, Park, Joo Yeon, Oh, Yu-Kyoung, 2013. Application of cationic liposomes for delivery of nucleic acids. *Asian J. Pharmaceut. Sci.* 8 (2), 72–80. <https://doi.org/10.1016/j.ajps.2013.07.009>.
- Soodaeva, S., Kubysheva, N., Klimanov, I., Nikitina, L., Batyrshin, I., 2019. Features of Oxidative and Nitrosative Metabolism in Lung Diseases. *Oxid. Med. Cell Longev.*
- Stratikopoulos, Elias E., Dendy, Meaghan, Szabolcs, Matthias, Khaykin, Alan J., Lefebvre, Celine, Zhou, Ming-Ming, Parsons, Ramon, 2015. Kinase and BET Inhibitors Together Clamp Inhibition of PI3K Signaling and Overcome Resistance to Therapy. *Cancer Cell* 27 (6), 837–851. <https://doi.org/10.1016/j.ccr.2015.05.006>.
- Thatikonda, S., Pooladanda, V., Sigalapalli, D.K., Godugu, C., 2020. Piperlongumine regulates epigenetic modulation and alleviates psoriasis-like skin inflammation via inhibition of hyperproliferation and inflammation. *Cell Death Dis.* 11, 1–17. <https://doi.org/10.1038/s41419-019-2212-y>.
- Thimmulappa, R.K., Chattopadhyay, I., Rajasekaran, S., 2019. Oxidative Stress Mechanisms in the Pathogenesis of Environmental Lung Diseases. *Oxidative Stress in Lung Diseases* 103–137. https://doi.org/10.1007/978-981-32-9366-3_5.

- Tian, Bing, Zhao, Yingxin, Sun, Hong, Zhang, Yueqing, Yang, Jun, Brasier, Allan R., 2016. BRD4 mediates NF-κB-dependent epithelial-mesenchymal transition and pulmonary fibrosis via transcriptional elongation. *Am. J. Physiol. Lung Cell. Mol. Physiol.* 311 (6), L1183–L1201. <https://doi.org/10.1152/ajplung.00224.2016>.
- Wang, H., Huang, W., Liang, M., Shi, Y., Zhang, C., Li, Q., Liu, M., Shou, Y., Yin, H., Zhu, X., Sun, X., Hu, Y., Shen, Z., 2018. (+)-JQ1 attenuated LPS-induced microglial inflammation via MAPK/NFkB signaling. *Cell Biosci.* 8, 1–15. <https://doi.org/10.1186/s13578-018-0258-7>.
- Wang, Jie, Lu, Ze, Wientjes, M. Guillaume, Au, Jessie L.-S., 2010. Delivery of siRNA therapeutics: barriers and carriers. *AAPS J.* 12 (4), 492–503. <https://doi.org/10.1208/s12248-010-9210-4>.
- Wang, J.Z., Zhang, R.Y., Bai, J., 2020. An anti-oxidative therapy for ameliorating cardiac injuries of critically ill COVID-19-infected patients. *Int. J. Cardiol.* 312, 137–138. <https://doi.org/10.1016/j.ijcard.2020.04.009>.
- Xu, J.M., Shi, G.P., 2012. Emerging Role of Mast Cells and Macrophages in Cardiovascular and Metabolic Diseases. *Endocr. Rev.* 33, 71–108. <https://doi.org/10.1210/er.2011-0013>.
- Yoshida, Y., Kumar, A., Koyama, Y., Peng, H., Arman, A., Boch, J.A., Auron, P.E., 2004. Interleukin 1 activates STAT3/nuclear factor-kappaB cross-talk via a unique TRAF6- and p65-dependent mechanism. *J. Biol. Chem.* 279, 1768–1776. <https://doi.org/10.1074/jbc.M311498200>.
- Yu, Hua, Pardoll, Drew, Jove, Richard, 2009. STATs in cancer inflammation and immunity: a leading role for STAT3. *Nat. Rev. Cancer* 9 (11), 798–809. <https://doi.org/10.1038/nrc2734>.